



TALLINN UNIVERSITY OF TECHNOLOGY

SCHOOL OF ENGINEERING

Department of Electrical Power Engineering and Mechatronics

# **INTEGRATED CURRENT MEASUREMENT SYSTEM FOR A SUPERCAPACITOR MODULE**

## **SUPERKONDENSAATORI MOODULI INTEGREERITUD ELEKTRIVOOLUMÕÕTMISSÜSTEEM**

MASTER THESIS

Student: Umut Güleğümüş

Student code: 201668MAHM

Supervisor: Saeed Rahimpour, Researcher

Co-supervisor: Siim Pille, Skeleton Technologies OÜ,  
Lead Capacitor Management System  
Engineer

Tallinn, 2023

*(On the reverse side of title page)*

**AUTHOR'S DECLARATION**

Hereby I declare, that I have written this thesis independently.

No academic degree has been applied for based on this material. All works, major viewpoints and data of the other authors used in this thesis have been referenced.

"19" May 2023

Author: Umut Güleğümüş

/signature /

Thesis is in accordance with terms and requirements

"19" May 2023

Supervisor: Saeed Rahimpour

/signature/

Accepted for defence

".....".....202... .

Chairman of theses defence commission: .....

/name and signature/

## **Non-exclusive Licence for Publication and Reproduction of Graduation Thesis<sup>1</sup>**

I, Umut Güleüngümüő hereby

1. grant Tallinn University of Technology (TalTech) a non-exclusive license for my thesis Integrated Current Measurement System for a Supercapacitor Module,

supervised by Researcher Saeed Rahimpour,

1.1 reproduced for the purposes of preservation and electronic publication, incl. to be entered in the digital collection of TalTech library until expiry of the term of copyright;

1.2 published via the web of TalTech, incl. to be entered in the digital collection of TalTech library until expiry of the term of copyright.

1.3 I am aware that the author also retains the rights specified in clause 1 of this license.

2. I confirm that granting the non-exclusive license does not infringe third persons' intellectual property rights, the rights arising from the Personal Data Protection Act or rights arising from other legislation.

19/05/2023

---

<sup>1</sup> The non-exclusive licence is not valid during the validity of access restriction indicated in the student's application for restriction on access to the graduation thesis that has been signed by the school's dean, except in case of the university's right to reproduce the thesis for preservation purposes only. If a graduation thesis is based on the joint creative activity of two or more persons and the co-author(s) has/have not granted, by the set deadline, the student defending his/her graduation thesis consent to reproduce and publish the graduation thesis in compliance with clauses 1.1 and 1.2 of the non-exclusive licence, the non-exclusive license shall not be valid for the period.

## ABSTRACT

*Author:* Umut Güleğümüş

*Type of the work:* Master Thesis

*Title:* integrated current measurement system for a supercapacitor module

*Date:* 19.05.2023

*56 pages (the number of thesis pages including appendices)*

*University:* Tallinn University of Technology

*School:* School of Engineering

*Department:* Department of Electrical Power Engineering and Mechatronics

*Supervisor(s) of the thesis:* Researcher Saeed Rahimpour

Siim Pille, Skeleton Technologies OÜ, Lead Capacitor Management System Engineer

*Abstract:*

Supercapacitor modules use state of health monitoring for remaining supercapacitor lifetime detection. Accurate current sensing is required for detecting state of health. For this purpose, a low-cost and easy-to-implement current sensing method is explored. The method involves using an existing terminal busbar of the module as a current sensing shunt resistor. The main advantages of the proposed solution is no added shunt resistor, meaning no resistor cost and no increase in total resistance. Simulations and tests results show that the proposed solution is viable, with requirement of a calibration procedure that can be implemented in serial production environment.

*Keywords:* supercapacitor module, state-of-health, current sensing, busbar, shunt resistor, current sense amplifier, calibration

# LÕPUTÖÖ LÜHIKOKKUVÕTE

*Autor:* Umut Güleüngümüŝ

*Lõputöö liik:* Magistritöö

*Töö pealkiri:* superkondensaatori mooduli integreeritud elektrivoolumõõtmisüsteem

*Kuupäev:*

56 lk (lõputöö lehekülgede arv koos lisadega)

19.05.2023

*Ülikool:* Tallinna Tehnikaülikool

*Teaduskond:* Inseneriteaduskond

*Instituut:* Elektroenergeetika ja mehhatroonika instituut

*Töö juhendaja(d):* Teadur Saeed Rahimpour

Siim Pille, Skeleton Technologies OÜ, Kondensaatorite juhtimissüsteemi juhtiv insener

*Sisu kirjeldus:*

Superkondensaatori moodulid hindavad oma seisundit, et tuvastada, kui palju on moodulil veel eluiga alles. Seisundi tuvastamiseks on vaja täpset vooluandurit. Sel eesmärgil uuritakse odavat ja lihtsalt rakendatavat vooluanduri kontseptsiooni. Kontseptsioon hõlmab moodulis olemasoleva voolulati kasutamist voolu mõõtvana šunditakistina. Kavandatava lahenduse peamised eelised on see, et ei ole lisatud lisa šunttakistit, mis tähendab, et hind ei suurene ning mooduli kogutakistus ei suurene. Simulatsioonid ja katsetulemused näitavad, et pakutud lahendus on lubav, kui kasutada kalibreerimist seeriatootmises.

*Märksõnad:* superkondensaatori moodul, mooduli seisund, vooluandur, voolulatt, šunditakisti, voolumõõtmise võimendi, kalibreerimine

# THESIS TASK

Thesis title in English: **Integrated Current Measurement System for a Supercapacitor Module**

Thesis title in Estonian: **Superkondensaatori Mooduli Integreeritud Elektrivoolumõõtmisüsteem**

Student: **Umut Gulengumus, 201668MAHM**

Programme: **MSc Mechatronics**

Type of the work: **Master Thesis**

Supervisor of the thesis: **Saeed Rahimpour, Researcher**

Co-supervisor of the thesis: **Siim Pille, Skeleton Technologies OÜ, Lead Capacitor Management System Engineer, siim.pille@skeletontech.com**  
(company, position and contact)

Validity period of the thesis task: **2022/2023 2022/2023 Spring**

Submission deadline of the thesis: **18/05/2023**

---

Supervisor (signature)

---

Student (signature)

---

Head of programme (signature)

---

Co-supervisor (signature)

## 1. Reasons for choosing the topic

Supercapacitor modules are multiple-cell arrangements that are built to provide higher capacitance and voltage values by connecting individual cells in series and/or parallel arrangements. Similarly to Li-ion battery modules, an energy storage management system is used for balancing to compensate for differing cell performances.

SOH (State of Health) is an important group of parameters including voltage, current and ESR (equivalent series resistance) that is an indicator of estimated lifetime duration of a supercapacitor module. The aging process of a supercapacitor occurs due to degradation of its performance in storing and delivering a certain amount of charge [1]. In a direct SOH prediction method, a correct measurement of the current during the cyclic operation of the supercapacitors is required [2]. As current is highly affected by temperature, a need for an candidate for a different type of Online, low-cost

Busbars are conductors that are used in a supercapacitor module for series and parallel

connection of cells as well as the main terminals. They are mostly monomaterial, made of aluminium or copper and have rectangular or circular cross-sections. Main reason for their ubiquity is the very low resistance and low cost. In this thesis work, a current measurement system will be built on a terminal busbar, which is expected to yield a low-cost solution, due to eliminating the need of using an additional series Shunt resistor. Since a serially produced busbar will have geometric and material tolerances, and a resistivity that is highly temperature-dependent, such a method should have following functionalities:

- current measurement method which can compensate for the varying temperature effects is valid.
- Calibratable, in order to correct for material and component manufacturing tolerances

Using a Shunt resistor for current measurement in a supercapacitor module has below drawbacks

- Shunt resistors are specialized components and costly
- A series connected resistor increases the ESR of a module. Most modules are in the order of single-digit mOhms.
- Adding a Shunt resistor occupies packaging space inside a module.
- A Shunt resistor's resistance is temperature-dependent.

In light of the above mentioned drawbacks of the conventional method, any system that utilizes supercapacitors can benefit from a lower ESR and a cheaper current measurement method.

## **2. Thesis objective**

This thesis study aims to provide a reliable and cost-effective electrical current measurement method for a supercapacitor module, with no increase in ESR. The target measurement error is 0.5% across the current interval. This method is expected to provide an alternative to the common shunt resistor usage for current measurement, which undesirably increases the ESR of a module.

## **3. List of sub-questions:**

- Analysis of full signal chain error due to busbar and measurement electronics
- What is the accuracy of measured current along a 30 mm-wide aluminium busbar?

- How much the varying temperature of aluminium busbar affect the accuracy of the current measurement? How can the temperature of the busbar be used to compensate for errors?
- What is a simply and low-cost temperature measurement method of a busbar to generate temperature data for current measurement?
- How does material and geometric variances due to manufacturing affect the accuracy and repeatability of the mentioned current measurement method?

#### **4. Basic data:**

- Voltage drop between measurement points along the reference busbar
- Effective resistance between measurement points along the reference busbar at operating temperature interval of the SC module
- Average temperature of the measured segment of the reference busbar at operating temperature interval of the SC module
- Reference current measurement data obtained with industry-standard device to compare with the method data
- Repetition of initial three data collections with different busbar specimens
- Error sources from the current sensing components being used for current measurement

#### **5. Research methods**

- Research and analysis for theoretical error sources across the current-sensing circuit pathway
- Accuracy analysis of the existing current sensing methods to create a baseline for comparison
- Initial reference current measurements via industry-standard device
- Modeling and simulation of heat generation and electrical current in busbar
- Determination of the measurement spots for current and temperature on the busbar. Temperature monitoring of busbar under load via IR camera.
- Integration of measurement PCB with busbar according to simulation results and test results
- Formulation of the temperature-resistance dependency of the busbar and using this dependency to compensate for the errors across the operating current interval
- Incorporating all current sensing circuit and electronic component errors to current sensing algorithm for correction

- Finalization of the prototype, tests and results

## 6. Graphical material

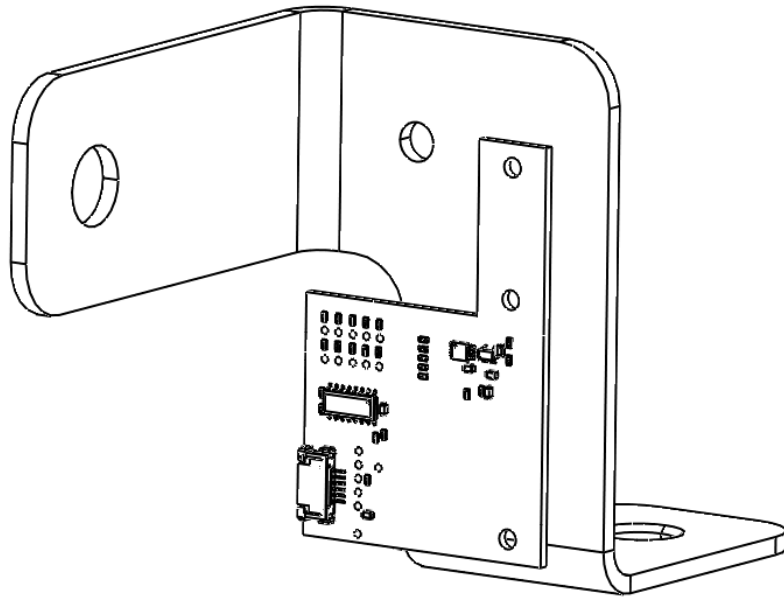


Figure 6.1 A representative illustration of busbar connected to PCB at measurement points

As shown in Figure 3.1, the busbar will be attached on PCB via rivets. The temperature and voltage readings will be done via rivets. Locations of these rivets are critical, as accurate measurement will depend on them.

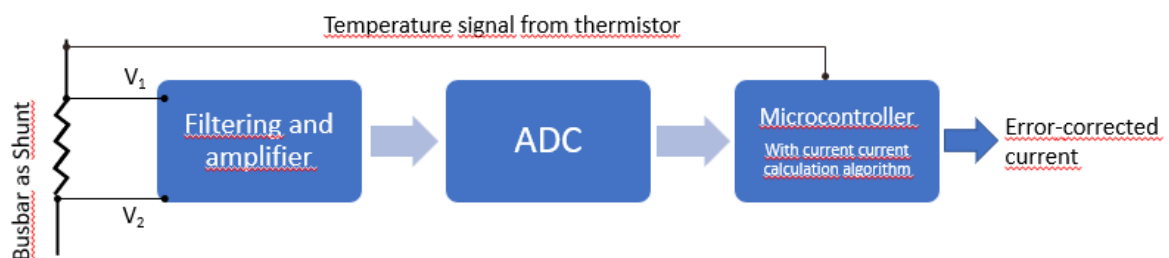


Figure 6.2 FBD of current sensing method

## 7. Thesis structure

**Chapter 1:** A brief introduction with the definition of problem statement, results significance and motivation is explained. The background for SOH and current measurement methods for energy storage systems is explored.

**Chapter 2:** The stages of current measurement method design is documented.

**Chapter 3:** The results and analysis of the results are given.

**Chapter 4:** Conclusion of the thesis study.

## 8. References

[1] D. Torregrossa, M. Paolon, "Modelling of current and temperature effects on supercapacitors ageing. Part II: State-of-Health assessment", Journal of Energy Storage, Volume 5, 2016, pp. 95-101.

[2] N. V. Vakrilov and N. M. Kafadarova, "A Review of Supercapacitors State of Health Estimation Methods," 2022 XXXI International Scientific Conference Electronics (ET), 2022, pp. 1-5, doi: 10.1109/ET55967.2022.9920314.

[3] "How Do Busbars Work And What Are They Used For?" <https://blog.prv-engineering.co.uk/what-are-busbars-used-for/> (accessed October 01, 2022).

[4] „Determining the Equivalent Series Resistance (ESR) of Capacitors" <https://www.allaboutcircuits.com/technical-articles/determining-equivalent-series-resistance-esr-of-capacitors/#:~:text=The%20current%20produces%20a%20voltage,measured%20voltage%20by%20the%20current.> (accessed October 01, 2022).

## 9. Work stages and schedule

Activity	Time frame (2023)
Literature review	March
Modeling and simulation	March-April
Measurement setup design	April - May
Busbar integration and tests	May

*Terms of thesis closed defence and/or thesis restricted access conditions to be formulated on the reverse side*

# CONTENTS

ABSTRACT .....	4
LÖPUTÖÖ LÜHIKOKKUVÕTE .....	5
THESIS TASK .....	6
LIST OF ABBREVIATIONS AND SYMBOLS .....	13
INTRODUCTION .....	14
1. LITERATURE REVIEW .....	16
1.1 Existing methods of current sensing .....	16
1.1.1 Current sensing by a shunt resistor .....	16
1.1.2 Current sensing by current transformer .....	18
1.1.3 Current sensing by Hall effect sensor .....	18
1.1.4 Current sensing by Fluxgate sensor .....	19
1.2 Comparison of the current sensing methods and conclusion .....	19
1.3 Aims of the thesis .....	21
2. METHOD .....	22
2.1 Description of the module and its components .....	22
2.2 Setup of the current measurement solution .....	22
2.2.1 Error sources .....	26
2.3 Simulation results .....	30
2.4 Test setup and measurements at different currents .....	35
2.4.1 Test Setup .....	35
2.4.2 Measurement results .....	38
2.5 Calibration method .....	45
3. RESULTS .....	48

SUMMARY .....	51
KOKKUVÕTE .....	53
LIST OF REFERENCES .....	55

## **LIST OF ABBREVIATIONS AND SYMBOLS**

SoH – State of Health

ESR – equivalent series resistance

PCBA – printed circuit board assembly

MCU – *micro controller unit*

$v$  – voltage

V – volt

$I$  – electrical current

$R$  – electrical resistance

$\Omega$  – Ohm

A – ampere

DC – direct current

AC – Alternating current

$P$  – power

CM – common-mode

$G$  – gain

$\alpha$  – temperature coefficient of resistance

Al – Aluminum

T – temperature

TDS – technical data sheet

CSA - current sense amplifier

ppm - parts per million

K – Kelvin

RSS – root-sum-square

SS – steady-state

PSU – power supply unit

DAQ – data acquisition device

# INTRODUCTION

Electrical current measurement or current sensing is a widely utilized functionality in many different types of equipments from battery management systems to electric motors. The purpose of knowing and tracking the electrical current may serve to different end goals. These goals might be state of health measurement of an energy storage system, or performance or safety monitoring of other types of equipments.

Supercapacitors are a type of energy storage solution that store energy in the form of electrostatic charge. Also sometimes termed as ultracapacitors, they differ from regular capacitors by their high capacitance, which is thanks to their electrostatic double-layer structure. Unlike Li-ion batteries, they do not store energy chemically, which grants them higher number of charging-discharging cycles over their usable lifetime. Most important characteristics are higher power density and lower energy density, compared to Li-ion and other widespread energy storage solutions. Utilization of supercapacitors is similar to conventional battery packs, in that, a battery management system is employed to combine multiple cells in order to get higher voltage and energy values.

SoH is an important lifetime indicator of supercapacitors derived based on voltage, current and ESR. The aging process of a supercapacitor occurs due to degradation of its performance in storing and delivering a certain amount of charge [1]. The conventional method for onboard SoH monitoring involves accurate current measurement via Shunt resistors. Shunt resistors are specialized components that characteristically feature an accurate and relatively constant resistance. This feature helps to reduce the errors in a current measurement solution. In this thesis study, the feasibility of a cheaper and simpler alternative to using a shunt resistor is explored. Error sources, tests results, compensation of these errors and a robust calibration method that can be applied in serial production setting will be documented.

The product which is the subject of the research in this thesis study is currently under development by Skeleton Technologies OÜ. It is named as „162V module“ and is aimed towards industrial applications such as electrical grid stability and mining. The module is designed in a typical supercapacitor module structure, which includes cellpack, signal and power connections, capacitor management system and other structural parts.

DewesoftX, Ansys and Altium are the software packages that are used in this thesis study.

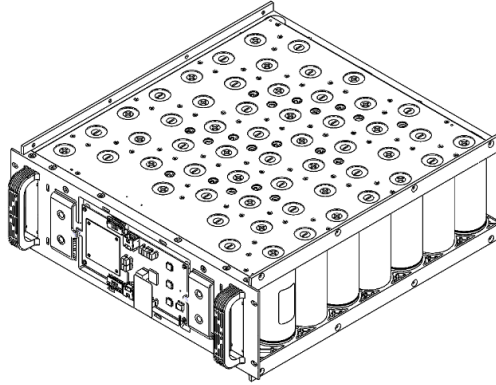


**Figure 1.1** 162V supercapacitor module

The thesis main body is structured as follows:

1. Literature review
2. Method
3. Results

Keywords: supercapacitor module, state-of-health, current sensing, busbar, shunt resistor, current sense amplifier, calibration

# 1. LITERATURE REVIEW

In this chapter, an overview of the commonly used current measurement methods will be given. The methods will be compared in terms of applicability, cost, accuracy. A conclusion will be made and justification for choosing the selected current measurement will be provided. Finally the aims of the thesis will be presented.

## 1.1 Existing methods of current sensing

Current sensing is an essential part of many different types of electrical devices. It is important to know the amount of the electrical current because it ensures the proper operation of the device. Moreover, it is an important aspect for performance tracking and safety monitoring. There are mainly four different techniques used in current sensing in industrial applications. These are

1. Current sensing by Shunt resistor (based on Ohm's law)
2. Current transformer (based on Faraday's law of induction)
3. Hall effect sensor (based on Hall effect)
4. Fluxgate sensor (based on Hall effect)

There are several more techniques such as Rogowski coil and Magneto-resistive current sensor, which are based on Faraday's law of induction and magnetic fields, respectively. However they will not be examined within the scope of this thesis study, as only the relatively simple and low-cost options are shortlisted here.

### 1.1.1 Current sensing by a shunt resistor

Current sensing shunt resistors are specially designed resistors used specifically for current measurement. The main characteristics are relatively low resistance (mostly in the order of 10 mΩ) [2] and low tolerance. The shunt resistor is connected in series to a circuit. The method involves measuring the voltage drop across the shunt resistor, usually via a differential amplifier. Knowing the resistance of the shunt resistor, measured voltage gives the electrical current via Ohm's law

$$I = v/R [15] \tag{1.1}$$

Even though current sensing by a shunt resistor is the simplest and easy to implement, it comes with some drawbacks. Firstly, to have a reliable low resistance, a large-size resistor is required. This brings packaging issues in devices where size and weight matters. Secondly, there is a temperature drift on the resistance value, though lower temperature coefficients are possible with costly high-precision shunt resistors. Another drawback is the requirement to amplify the voltage difference across the Shunt resistor. This is also followed by an analog-to-digital converter on the signal chain. Lastly, being connected in series, there will always be some loss of power through the shunt resistor, which is dissipated as heat.

The selection for the resistance value of a shunt resistor is determined as a compromise between good accuracy at lower currents vs low power dissipation at higher currents. Having a low resistance is directly proportional to the power loss from the circuit. If a lower resistance is selected to combat this, as the signal chain has many sources of error, the smaller resistance will result in lower or unusable accuracy at low current range. This is because, measurement errors such as noise and amplifier offset voltage has a higher impact on the actual measured voltage, at low currents as the useful signal is quite low value as well.

**Current sensing by trace resistance** (based on Ohm's law) is an iteration of current sensing via shunt resistor, where shunt resistor is omitted, and a segment of copper trace on a PCB is utilized instead. This method appears highly simplistic and cost effective, however there are significant drawbacks which disqualifies it to be used in high-accuracy applications. Main problem with using PCB Copper trace is that the Copper trace is highly prone to variations in the PCB manufacturing process. To have a relatively reliable resistance that can handle large currents (more than 10 A), a very large continuous trace should be used. However this brings packaging issues in PCB's where space is limited [3]. Furthermore, even with a large enough trace, further difficulties arise when currents as high as 1000 A are applied.

### 1.1.2 Current sensing by current transformer

Current transformer's working principle is based on a transformer. It is a passive device that converts a high primary current to a lower secondary current. It is mainly used in AC applications. Due to containing windings similar to voltage transformers, it takes up significant volume. They are not suitable for DC applications [4].



**Figure 1.1** Current transformer

### 1.1.3 Current sensing by Hall effect sensor

Hall effect sensors are one of the two aforementioned sensors based on magnetic field sensing, the other being fluxgate sensor. Hall sensors create an analog output voltage, which is proportional to the detected magnetic field. Amplification for the output signal is necessary. Although these devices are small and low-cost, they are susceptible to magnetic stray fields [5].



**Figure 1.2** Hall effect current sensor [6]

### 1.1.4 Current sensing by Fluxgate sensor

This method employs a saturable inductor which is induced by the magnetic field created by the primary current. It is widely used in the monitoring and Control of various electronic products, and is the most sensitive and reliable solution among the current sensing technologies. Despite the favorable accuracy, it is limited to small currents and is relatively costly [5].

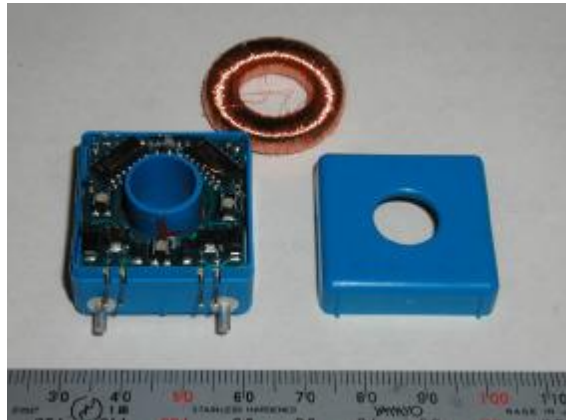


**Figure 1.3** Fluxgate current sensor [7]

## 1.2 Comparison of the current sensing methods and conclusion

Table 1.1 provides a comparison of the given current sensing methods. Current transformer is automatically eliminated as the studied application current is DC. Since supercapacitors modules come in many different sizes and with many modules packaging space is an issue due to energy density targets, a light-weight and small-sized solution is desired. Cost is another factor as with all mass-produced products, hence a low-cost solution is desired. For its simplicity and low cost, current sensing via shunt resistor is deemed ideal for this study, despite isolation risks and temperature dependency.

**Table 1.1** Comparison of different current sensing technologies [4]

	Pros	Cons
Shunt resistor	Low complexity, wide bandwidth	Power dissipation, no isolation, self-heating
Current transformer	Passive device	Only suitable for AC
Hall-effect sensor	Isolation, no power losses	Susceptible to stray magnetic fields, temperature dependent offset, limited accuracy
Fluxgate sensor	Isolation, no power losses, good accuracy	Disturbance due to excitation frequency, large operation current, limited bandwidth w/o additional transformer, cost

Having chosen shunt resistor method, a problem arises after a brief market check. A shunt resistor that is capable of handling 2 kA is required for the 162V module. A close contender that is capable of 1.4 kA is at a price of ~30 €/unit [16]. This is a high cost for a serial production module. Furthermore another drawback comes from the addition of a resistive component to the circuit, causing additional power dissipation in accordance with formula

$$P = I^2 R \quad [15] \quad (1.2)$$

Naturally, addition of a resistive component to the circuit increases the total series resistance, which is termed as „equivalent series resistance“ (ESR) in a supercapacitor module. Supercapacitors have relatively low energy density, in contrast with their very high power density. Due to this, featuring a low ESR is essential for both higher power and stored energy ratings [7]. Most medium-sized supercapacitor modules feature an ESR of 1-10 mΩ. Considering a high-current capable shunt resistor is in the order of a couple hundred μΩ [16], the impact in the total ESR would be significant. This shows

that, adding a shelf product as a shunt resistor to the module would be both costly and detrimental to performance.

Using an inherent portion of circuit as a current-sensing shunt resistor has been considered in the past, although has a limited use in industry due to drawbacks. The method of using Copper trace as shunt resistor has already been mentioned in 2.1.1. This method proves to be inadequate for most applications that require high accuracy and high current, however, copper trace of a PCB is not the only inherent portion of a circuit. As exemplified in [4], busbars are standard components of many energy storage units, and can be considered as a shunt resistor alternative. Due their standard geometry and large cross-sectional area, busbars promise relatively low resistance and low power dissipation. Nevertheless, being aluminum or copper make them still susceptible to temperature effects.

### **1.3 Aims of the thesis**

The objective of this thesis study is to explore the usage of busbars in current sensing as an integrated shunt resistor, which is a novel idea for supercapacitor energy storage modules. Main advantages will be

- Omission of an additional shunt resistor by relying on an integral part of the device, eliminating additional cost
- Not increasing the ESR, thus not increasing power loss or decreasing maximum, pulse current capability

Main challenge will be is expected to be the accuracy of the current sensing. Inside of a supercapacitor is a high in electrical noise, and temperature dependency will have to be compensated for.

## 2.METHOD

### 2.1 Description of the module and its components

As presented in 1. Introduction, the subject of this study will be the module named „162V“ after its rated working voltage of 162 V. It will be designed to withstand peak current as high as 3.5 kA, while typical application pulses will be in order of hundreds of amperes

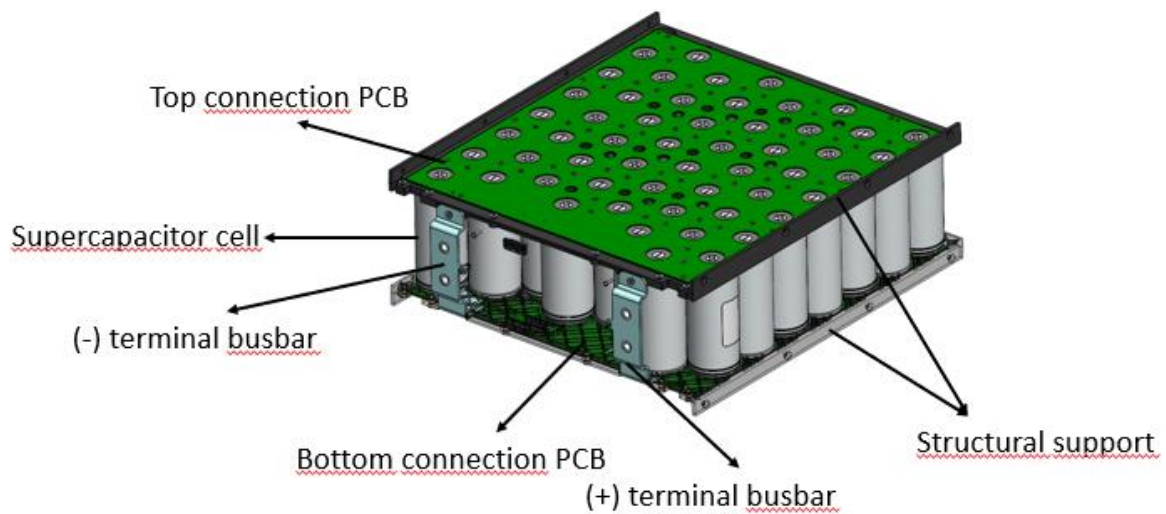


**Figure 2.1** Main components of 162V module

Figure 2.1 indicates the main components of the module. 54 cells are connected in series via cell busbars and the PCB's are connected to the busbars to carry various signals like voltage and temperature back to the CMS (capacitor management system) PCB. The balancer PCB and the cell busbars are not visible in Figure 2.1.

### 2.2 Setup of the current measurement solution

As the cells are connected in series circuit, the first question is which busbar to use as the shunt resistor. Figure 2.2 shows the 3 different busbars available. All are of aluminum EN AW-1050A and of 40x3 mm cross-section. At first glance, all seem to be suitable to be used as shunt resistor, based on their material and manufacturing tolerances. However, the voltage level of the shunt resistor is a factor on the accuracy of current sensing.

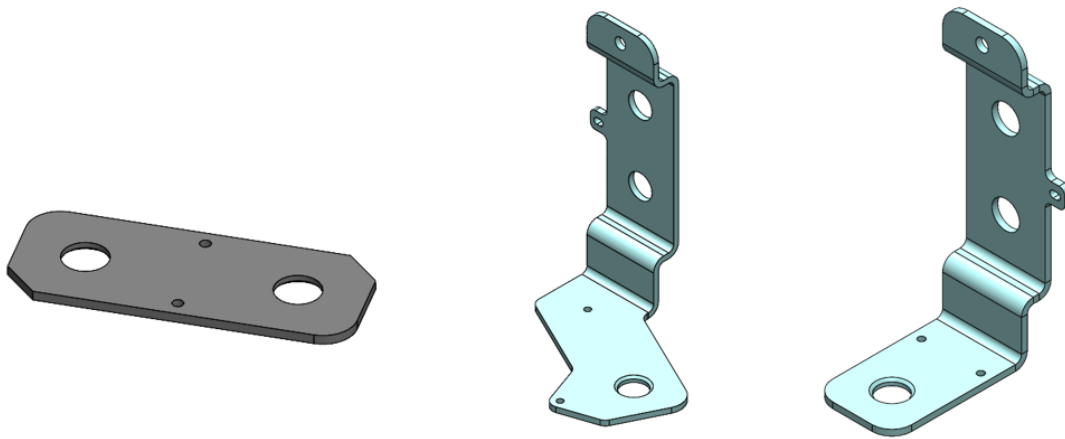


**Figure 2.2** From left to right: Cell busbar, (-) terminal busbar, (+) terminal busbar

In terms of the position in a circuit with respect to the load, shunt resistors are classified as low-side current sensing and high-side current sensing, indicated on Figure 2.3. The main challenge with high-side current sensing is the high common-mode voltage. Many current sensing devices (such as current sensing amplifiers) have limited CM voltage tolerance. Moreover, high-side placement add the CM noise, which tampers with sensing accuracy. Due to these effects, low-side placement will be used in this experiment setup.

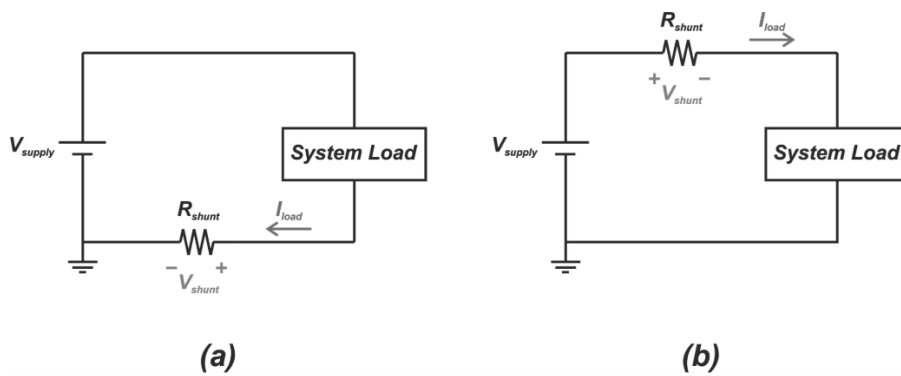


**Figure 2.3** (a) Low-side current sensing and (b) high-side current sensing techniques [9]

Figure 2.4 shows the bottom PCB and negative terminal busbar assembly. The busbar is attached to the PCB by rivets. The current sensing circuit is incorporated on the bottom PCB, and the busbar will act as the shunt resistor. Figure 2.5 indicates the main power supply spots, as well as the current sensing traces on the PCB layout. Although voltage measurement spots appear to be far away from the current path, a consistent effective resistance is expected and will be demonstrated by simulation in upcoming sections. Also to be noted is a thermistor which is placed close to the busbar to monitor the busbar temperature in order to correct for temperature-related changes on the busbar resistance.

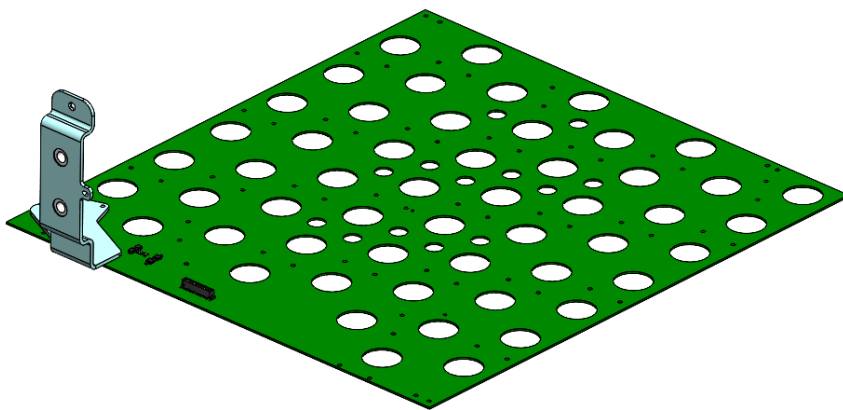


**Figure 2.4** Bottom PCB and negative terminal busbar

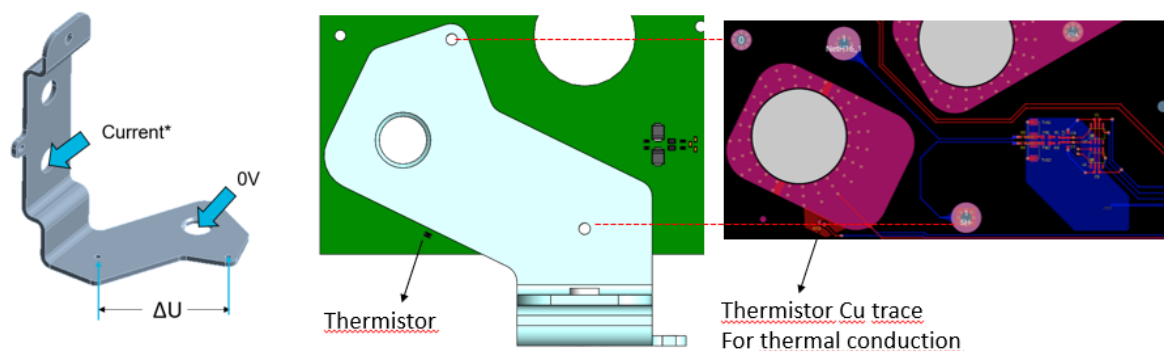


**Figure 2.5** Power supply points on busbar, voltage measurement points on busbar and PCB layout

The schematic for current sensing circuit is given in Figure 2.6 below. This design was created by the module development team, in accordance with the busbar current sensing plan which is the subject of this study. Visible from the schematic, at left hand side, two current sensing amplifiers are utilized. The reason for having two amplifiers is the different needs of gain ratios for high and low current magnitudes. The chosen amplifiers are INA240A3 and INA240A4. As their names imply, they are different versions of INA240 current sense amplifier, only the gain ratios being different at 100 and 200, respectively. A higher gain ratio is required to reduce the impact of noise at very low currents. For the rest of current spectrum, INA240A3 will provide the amplification. It is important that even at the highest operating current of 3.5 kA, the amplifier output should not be saturated. With the approximate resistance of the measured busbar segment at 10  $\mu$ A, the highest voltage drop would be 0.035 V. Amplifier output is given by equation (2.1)

$$v_{out,amplifier} = v_{ref} + G \times (v_{in+} - v_{in-}) \quad (2.1)$$

As our  $v_{ref}$  is chosen as  $v_{cc} / 2 = 2.5$  V, with gain ratio of 100, it follows that  $V_{out, amplifier}$  can reach as high as 6 V, in theory. In practice, this is not possible due to amplifier integrated circuit limitation of  $v_{out} < v_{cc}$ . In fact, for linear output, the output should be below the swing to  $v_{cc}$ . Acc. to [10], this gives 4.8 V. A maximum of 4.8 V output, while  $v_{ref}$  is 2.5 V indicates that the INA240A3 amplifier is able to sense to a maximum limit of 2.3 kA. As the developed module will have many different applications, this limit remains usable for some versions. Another benefit of setting  $v_{ref}$  to 2.5 V is the possibility to measure current at equal ranges during both charging and discharging (bi-directional).

Also noteworthy is that the supercapacitor module has bi-directional (charging and discharging) operation. Chosen current sense amplifier will allow current sensing in both directions.

Continuing on the description of the circuit schematic at Figure 2.6, at top left and bottom left two bypass filter is employed for reducing AC noise on the supplies of the current sensing amplifiers. From the sensing spots on the busbar into the inputs of both amplifiers, an input low-pass filter is available.

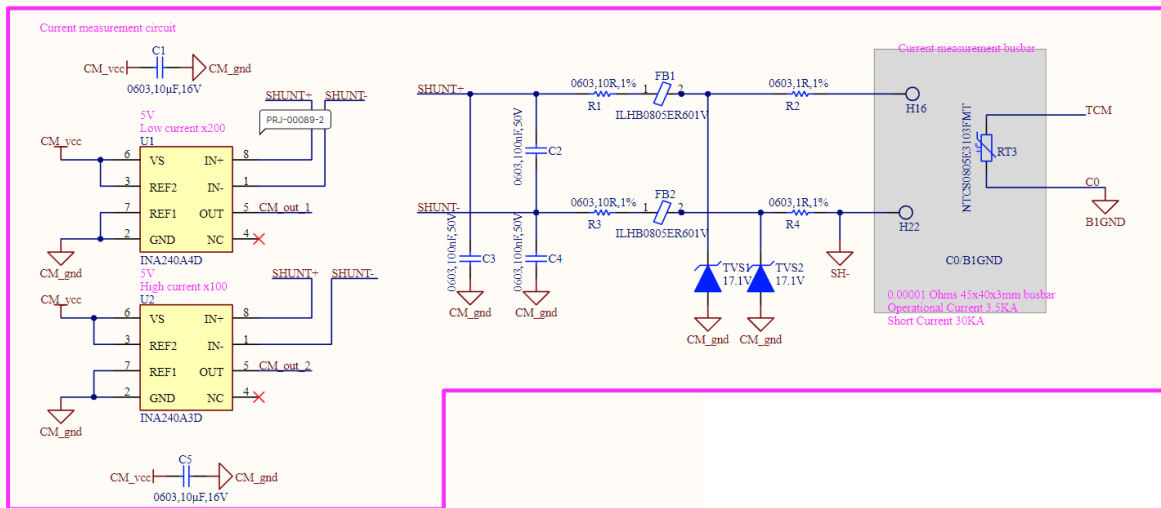


**Figure 2.6** Schematic of current sensing circuit

### 2.2.1 Error sources

In order to determine the error sources, one has to look for deviations, imperfections and sources of noise.

**Shunt errors** are two fold:

- Deviations from specimen to specimen, due to manufacturing tolerances and material impurities
- Temperature-dependency of resistance [10]

Even though these two pose high error percentages for an accurate measurement, fortunately, both errors can be significantly eliminated by calibrating. Figure 2.7 shows that until approximately 650°C, the electrical resistivity behaves almost linearly with temperature. This allows to define the resistance at a specific temperature T as follows

$$R(T) = R_0(1 + \alpha_{TK} (T - T_0)) \quad (2.2)$$

Where  $\alpha_{TK}$  is the temperature coefficient of Aluminum.

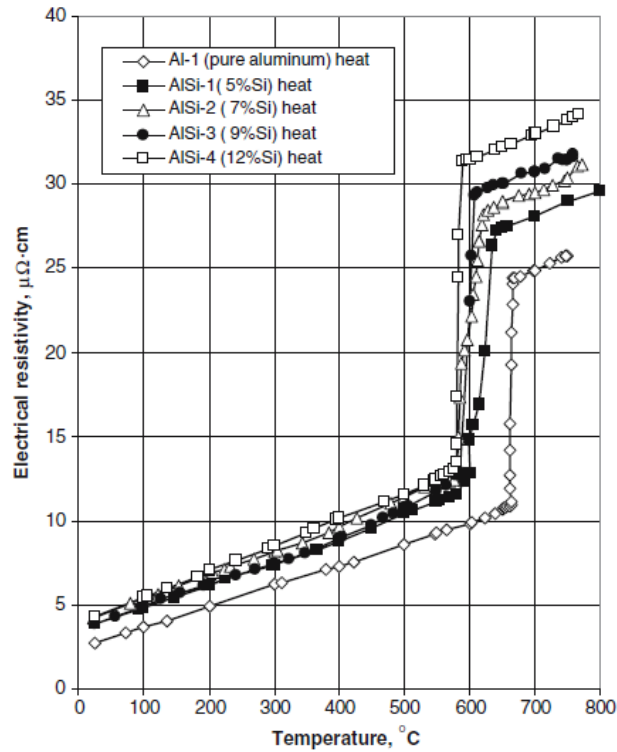


**Figure 2.7** Electrical resistivity of pure aluminum and binary AlSi Alloys [12]

**CSA (current sense amplifier) errors** stem from the architecture and manufacturing tolerances of the amplifier:

- amplifier input offset V
- amplifier input offset V T-drift
- amplifier gain error
- amplifier gain T-drift
- amplifier non-linearity error

From the TDS of the INA240A3, below maximum values are available [9]:

**Table 2.1** CSA errors [9]

<b>parameter</b>	<b>Max. value</b>	<b>unit</b>
Offset voltage, input-referred:	$\pm 25$	$\mu\text{V}$
Offset voltage drift	$\pm 250$	$\text{nV}/^\circ\text{C}$
Gain error	$\pm 0.20\%$	
Gain temperature drift	$\pm 2.5$	$\text{ppm}/^\circ\text{C}$
Non-linearity error	$\pm 0.01\%$	

As the input offset voltage acts as a constant throughout the entire input range, we expect it to dominate the total errors at low currents, and to become insignificant with increasing supply currents. The other errors will act uniformly across the entire supply current range.

The remaining error source is the temperature drift of the Al busbar. The temperature coefficient of Al resistance is  $0.403 /\text{K}$ . This means that, for a  $20^\circ\text{C}$  increase, we can expect  $\sim 8\%$  increase in the busbar resistance. For simplicity, the resistance can be assumed to change linearly with temperature, however, it is more realistic to use simulation data that was run at 4 different supply currents. Figure 2.8 shows the total RSS errors throughout 4 supply currents. RSS is used for a more realistic approach [13] From the graph, it is obvious that the a data obtained at these error specifications is not usable, and needs a correction algorithm. For comparison, in Figure 2.9, the specific error graph for CSA input offset voltage is given. It is apparent that this error type dominates until approximately 50 A, and diminishes further on.

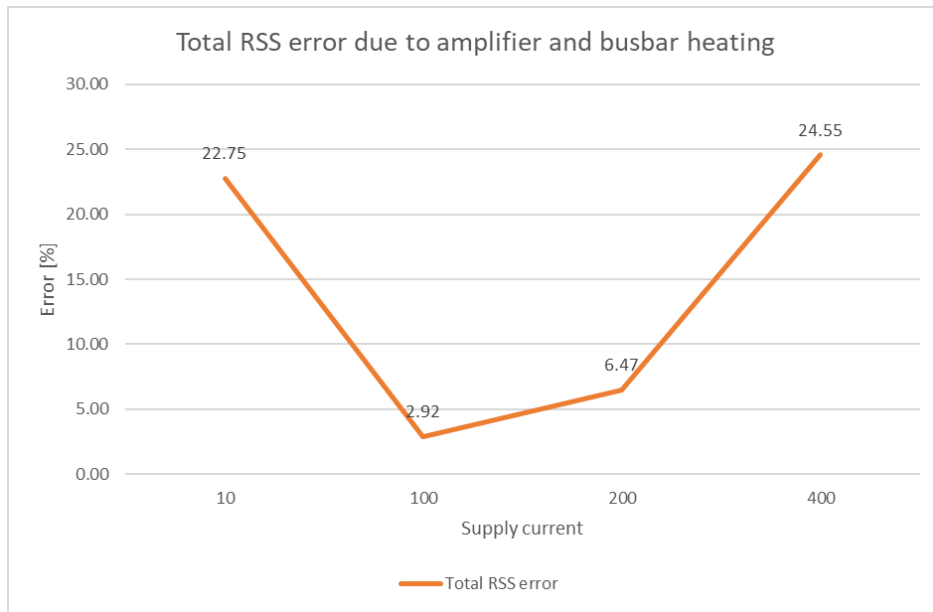


**Figure 2.8** Total RSS error due to amplifier and busbar heating

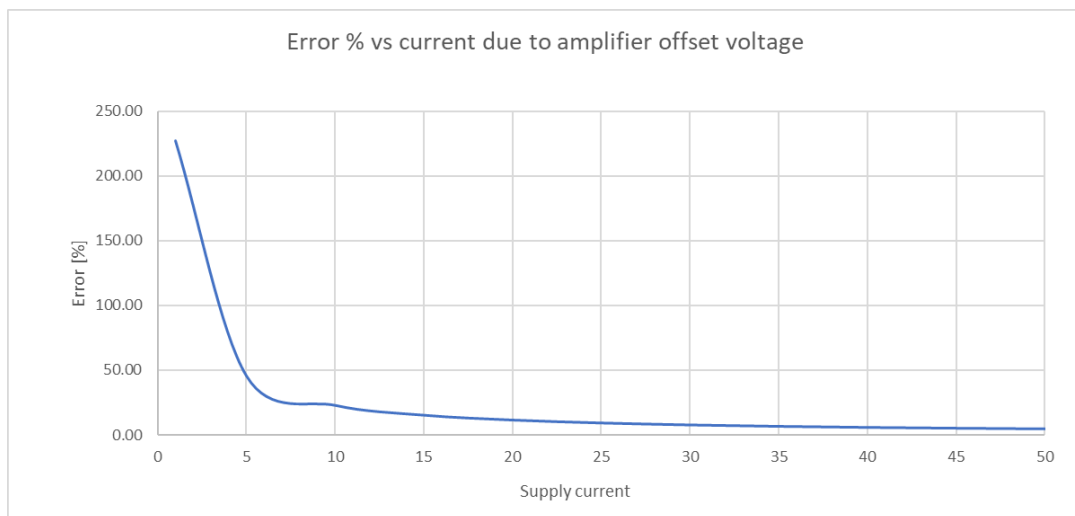


**Figure 2.9** %error vs current due to amplifier input offset voltage

**Other various sources of error** include:

- Thermo-electric voltages on the busbar
- Skin effect on the busbar
- EMI
- PCB layout

As these are difficult to estimate, they are out of scope for this study. However, good design practices should be followed to pro-actively avoid their effects.

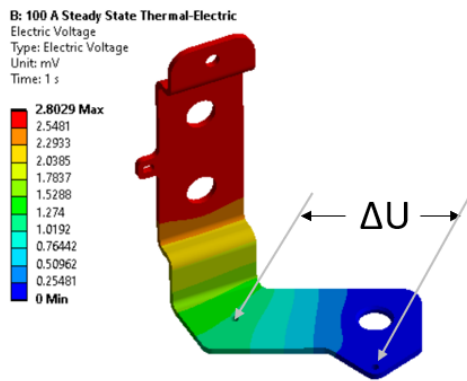
## **2.3 Simulation results**

Most shunt resistors are of uniaxial or prismatic geometry [14], which results in a predictable current pathway. With a complex geometry such as the busbar that is being used, it is necessary to see how the current, voltage and temperature propagates along the busbar, when a current is applied. To this end, several simulations were run, which will be presented in this section.

As it was indicated in Figure 2.5, the current inlet and exit points will be the same as the real-world usage. At 100 A and SS (steady-state), voltage drop and current density propagations were investigated. Ansys was used as the simulation solver. Figure 2.10 indicates the visualizations of the simulation results. From the voltage drop visualization, it is clear that the voltage propagation follows the current path (between current inlet and exit). Considering the max. voltage drop within the busbar is  $\sim 2.8$  mV and the drop across the measurement points is  $\sim 1.2$  mV, the measured segment still represents a significant portion of voltage drop within the busbar.

Current density visualization on the other hand, shows a significantly more complex color map. It can be seen that the current roughly follows the shortest path between current inlet and exit. A point to investigate here is, how similar it will be to temperature map of the busbar.

### Voltage Drop at 100A



### Current Density at 100A

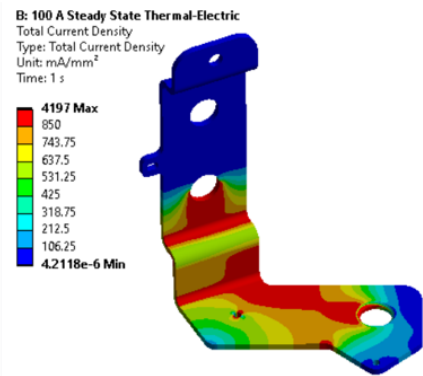


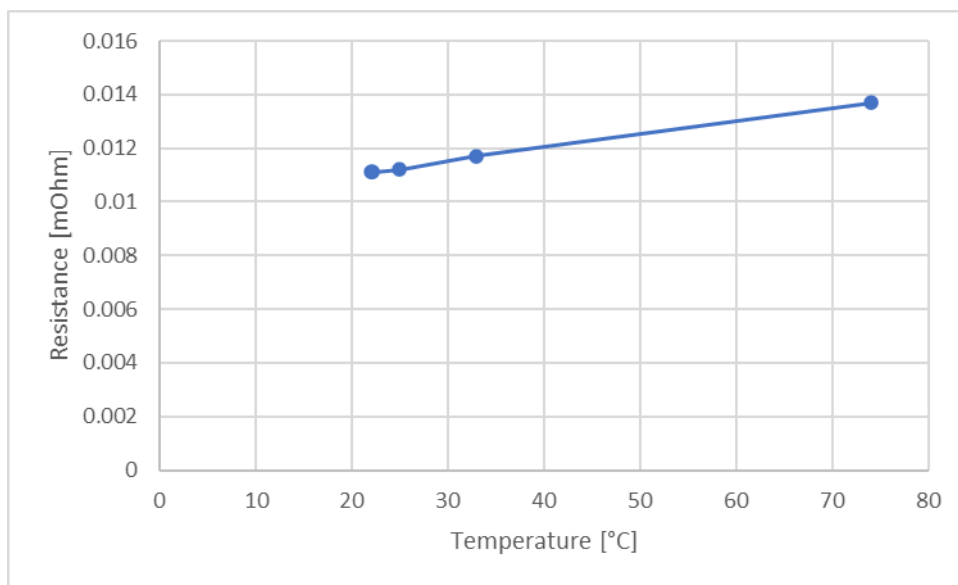
**Figure 2.10** Simulation results for 100 A SS current

**Table 2.2** Simulation results for 100 A SS current

Current [A]	Delta U [mV]	max. Voltage Meas. error [mV]	Ambient Temp [°C]	Busbar Temp [°C]	Res [mOhm]	Res increased [mOhm]	Voltage error due to Temp increase [%]	Current meas. Error [%]	Current meas. Error excl. temp [A]	Current meas. error incl. temp error [%]	Current meas. error excl. temp error [%]
1	0.01	0.0001	22	22	0.0111	0.0000	0.00	0	0.0050	0.5	0.5
10	0.11	0.0006	22	22.1	0.0111	0.0000	0.00	0	0.0500	0.5	0.5
100	1.12	0.0056	22	25	0.0112	0.0001	1.16	1.16	0.5000	1.7	0.5
200	2.33	0.0117	22	33	0.0117	0.0006	4.72	4.72	1.0000	5.2	0.5
400	5.48	0.0274	22	74	0.0137	0.0026	18.9	18.9	2.0000	19.4	0.5

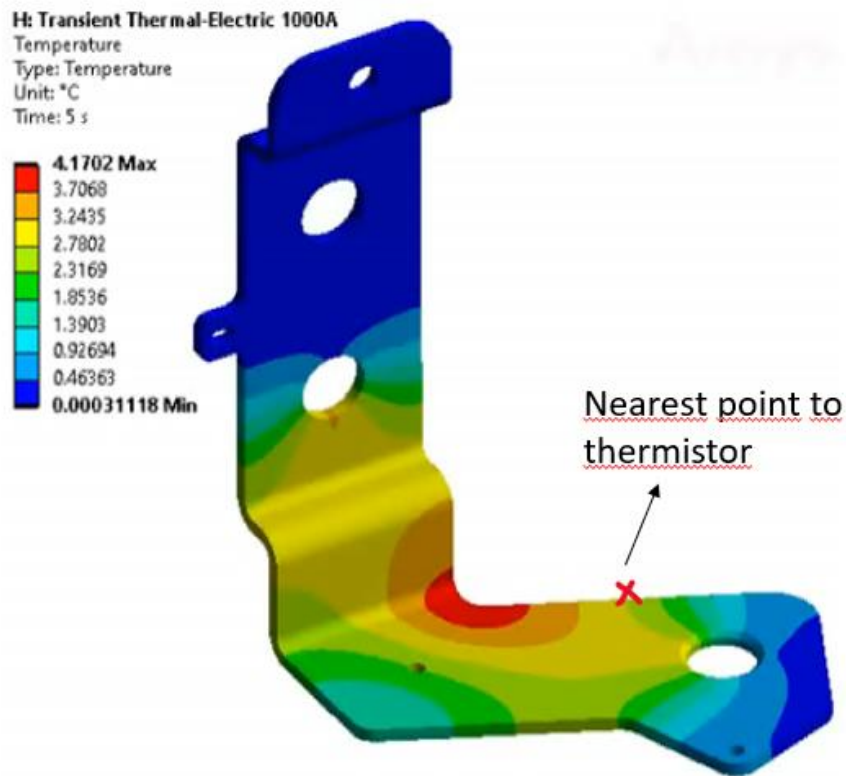
Table 2.2 summarizes the SS numerical results of 5 different current values. As expected, the SS temperature increases with applied current, which in turn increases the effective resistance. At 200 A and 400 A, the voltage error due to heating of the busbar is extremely high and indicates that a correction is required. As the current is measured indirectly by dividing the voltage drop to resistance, the current measurement error exactly follows the voltage error. It should be noted that these errors are calculated for a case where a fixed resistance at 22°C was assumed, neglecting the temperature effect on resistance.

Figure 2.11 depicts the relation of busbar resistance with temperature. As expected, the data follows a relatively linear path.



**Figure 2.11** Simulation results for 100 A SS current

Another important point is the temperature propagation in the busbar. Figure 2.12 shows a similar color map compared to the current density visual at Figure 2.10. This only makes sense, as the heat is the dissipated power, which is proportional to electrical current. As the temperature of the busbar will be monitored by a thermistor (introduced at 2.2), the accuracy of it is important for the overall current sensing accuracy. As the busbar and the copper trace leading to the thermistor has excellent thermal conductivity, no significant temperature gradient is expected at SS conditions. However, the time delay between effective temperature of the busbar segment and the thermistor temperature is worth investigating for transient cases. At Figure 2.12, there is  $\sim 2^{\circ}\text{C}$  difference at 5 seconds, for instance. Figure 3.13 indicates an increasing temperature difference exists at 1000 A transient case.



**Figure 2.12** Transient thermal map for 1000 A at 5 seconds

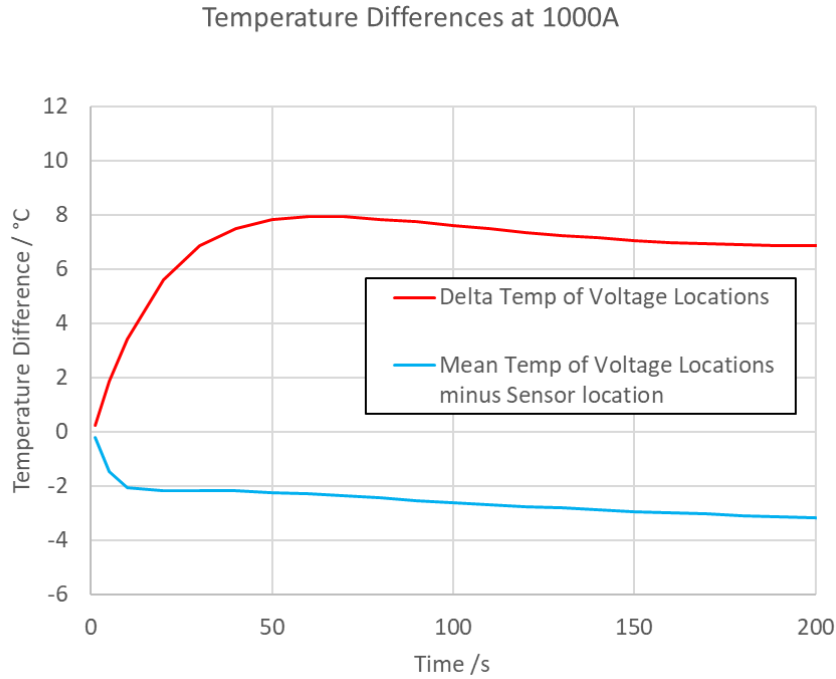


**Figure 2.13** Temperature differences at 1000 A (transient)

In conclusion, the simulation results indicate that a consistent effective resistance exists for the measured busbar segment. It is also in agreement with the known relation between Al resistivity and temperature. The results are promising for this method and real-world tests will be carried out at Section 2.4 to observe the performance.

## 2.4 Test setup and measurements at different currents

### 2.4.1 Test Setup

The tests were conducted in May 2023 in Skeleton Technologies testing facilities. Figure 2.14 depicts the tools that were used. Namely,

- ITech IT6006C-300-75 Bi-directional as power supply
- Dewesoft R8 as DAQ
- TENMA PSU 60V/3A/180W as auxiliary power supply

- DewesoftX as DAQ software
- Generic multimeter for on-the-spot measurements

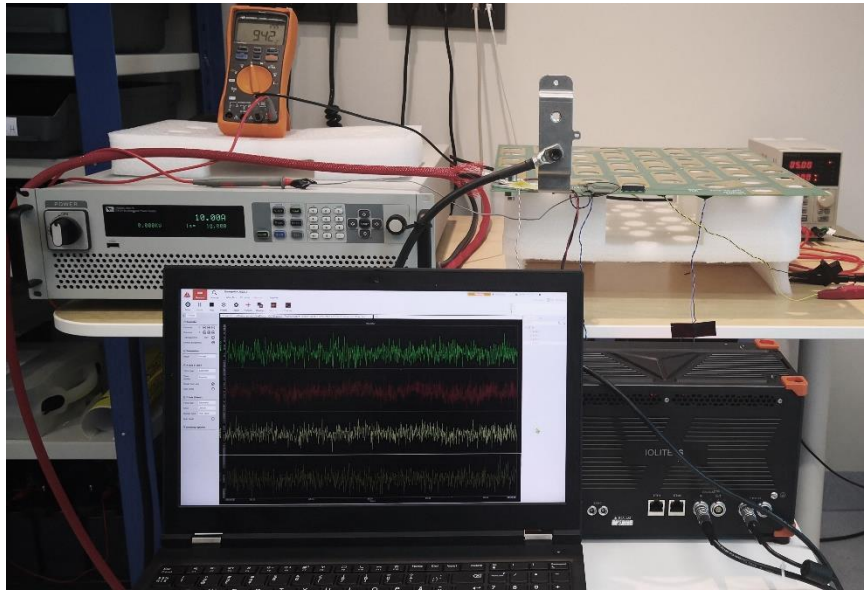


**Figure 2.14** Test setup

Below is the schematic for measurement circuit.

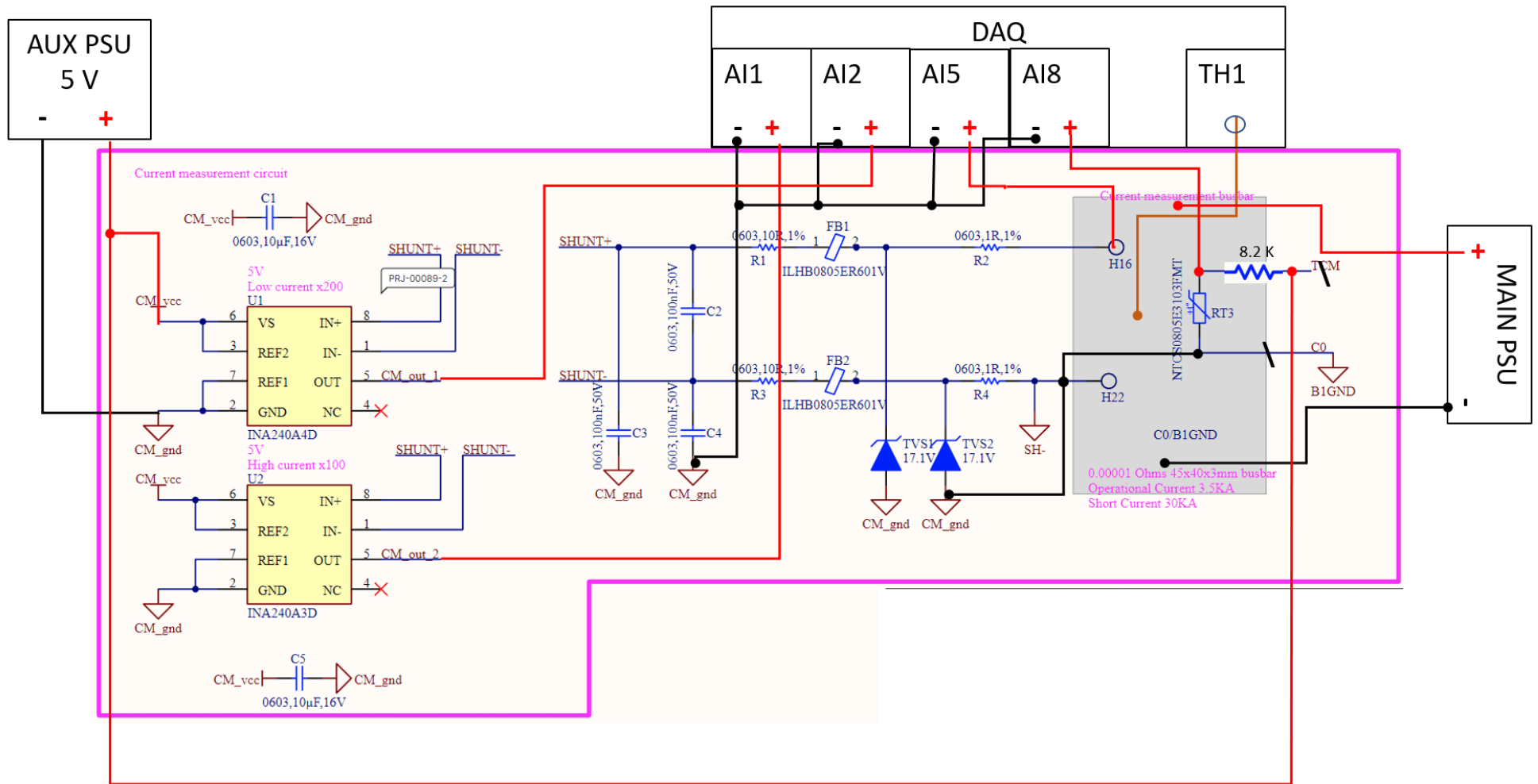
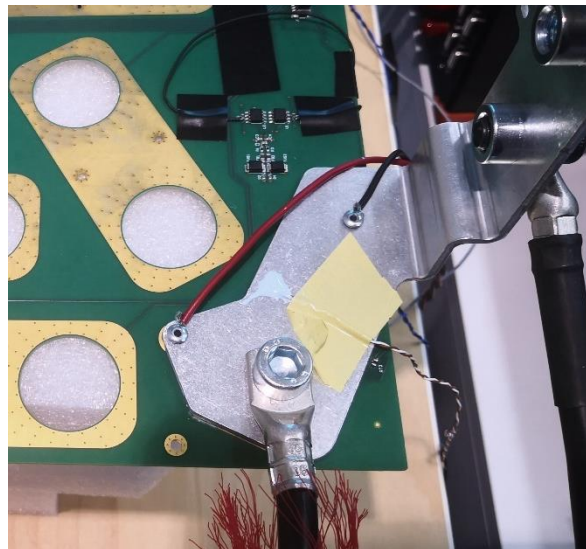


Figure 2.15 Schematic for measurement circuit

In this test setup, the main PSU substitutes for the charged cellpack, where normally the current comes from, during discharge mode. A realistic power cycle of the module would be charge-discharge cycle at 400 A. However, for the intention of validating the current sensing circuit, and due to device limits, max. current of 75 A will be applied. Similarly, the  $V_s$  that normally comes from balancer PCB by design, is supplied by an auxiliary PSU in this setup. As it can be seen from Figure 2.15, some adaptations/corrections were made to the original circuit. Firstly, via wire soldering, the H22 was connected to CM\_gnd (current measurement ground). Secondly, a voltage divider was applied to the RT3 via a 8.2 k $\Omega$  resistor and external voltage supply, in order to be able to measure the voltage drop across it. RT3 is the thermistor that will be used for temperature monitoring of the busbar. Finally, a thermocouple connection was made on the busbar, at the midpoint between two measurement points (Figure 2.16). All measurements are done on the DAQ.



**Figure 2.16** Close-up of the current measurement busbar with connections

### 2.4.2 Measurement results

Before starting the measurements 7 different supply current were selected within the main PSU capability, to analyze the current sensing performance. These currents are 10, 20, 30, 40, 50, 60 and 75 A. For reference, 0 A and 1 A were also added to the measurement plan.

**At 10 A transient supply**, it is clear that the input filter works satisfactorily, when the real V and amplifier outputs are compared. Figure 2.17 shows the exact time point of

current supply. The responses from the amplifiers are virtually instantaneous. At this session, the temperature fluctuated within  $0.02^{\circ}\text{C}$ , which is not surprising for such low power. This renders temperature effects insignificant. Similar responses were recorded for transient 60 A in Figure 2.18. From now on, we focus on the amplifier 2 output (200 gain) for simplicity.

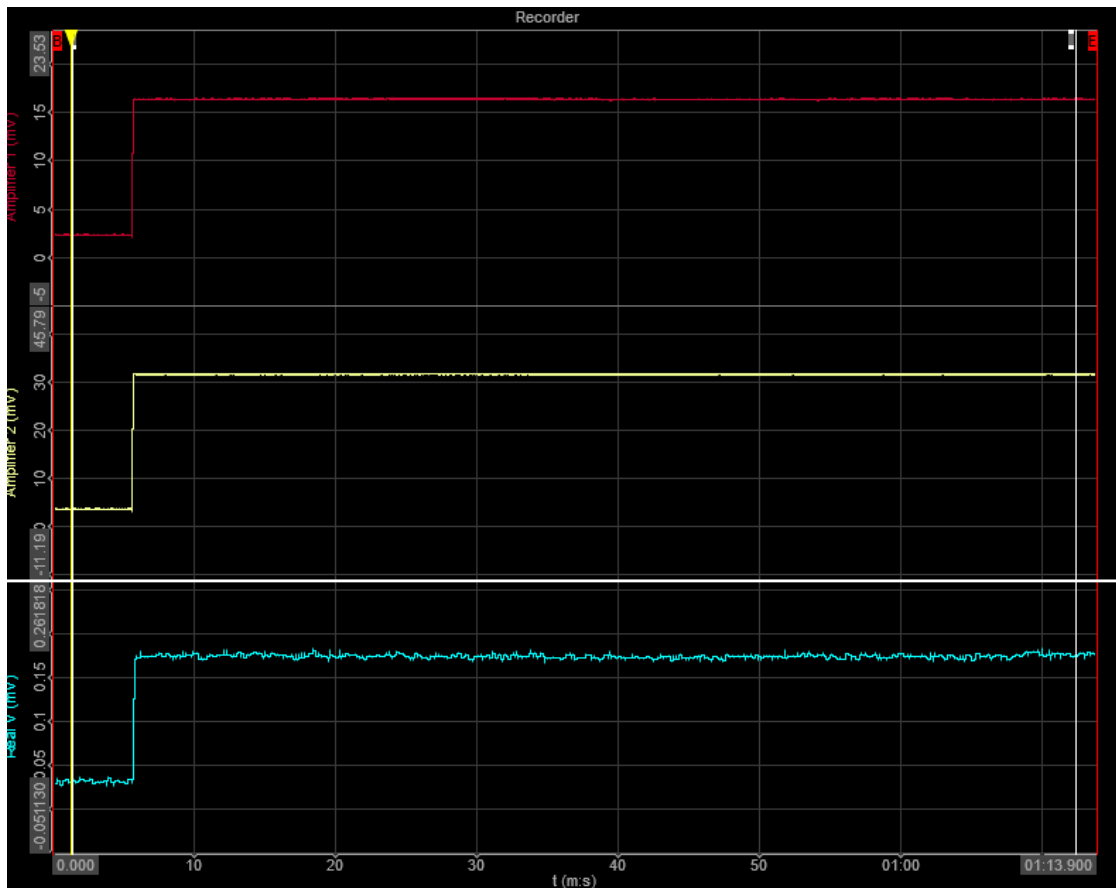


**Figure 2.17** Transient responses of voltage drop and amplifier outputs to 10 A current supply

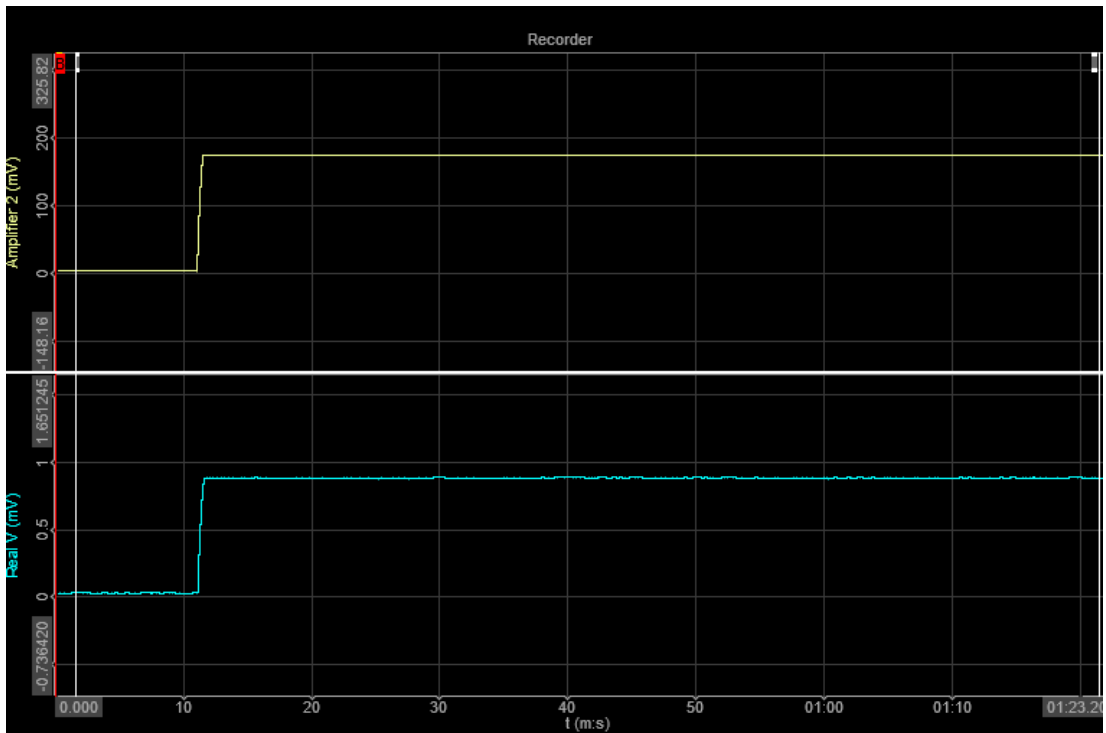


**Figure 2.18** Transient responses of voltage drop and amplifier 2 output to 60 A current supply

To analyze the results, a systematic approach has to be made. First, one must find out how the measured voltage changes with supplied current. Figure 2.19 shows that measured real voltage changes linearly with supply current. This is expected from Ohm's law. It should be noted that, in order to disregard the temperature effects, the average voltage values were not taken from entire session, but from the initial time portions, where temperature increased no more than 0.8°C. One must also take into consideration that, during the normal operation of current sensing, real voltage drop will not be monitored. The system will rely only on the CSA outputs.

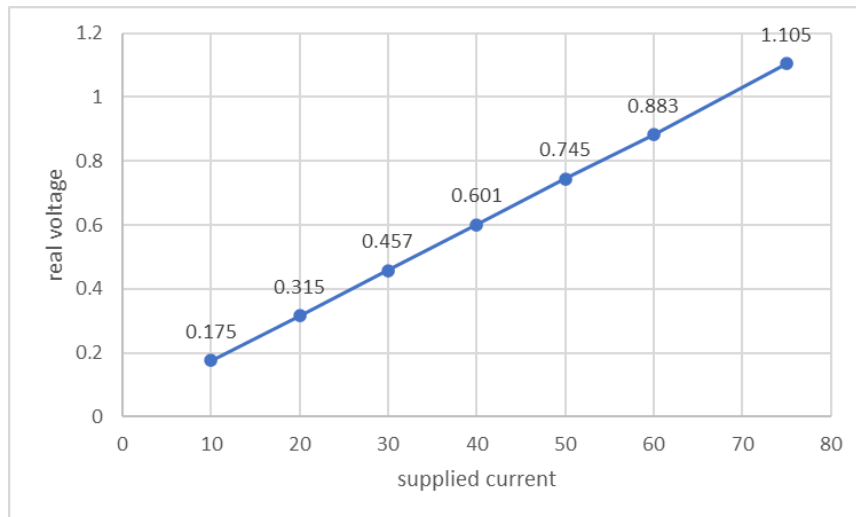


**Figure 2.19** Supplied current vs real voltage drop across busbar segment

Having validated the linearity of V-I, the next relation to explore is the gain ratio with supply current. Figure 2.20 shows that there is a predominantly increasing, but nonlinear trend to the gain ratio. Considering the nominal gain ratio of 200, the lower values at low currents can be explained by the input offset voltage of the amplifier. As there is still a percentage error of 1.14 at 100 A according to Figure 2.9 and [9], the input offset voltage can be the reason for not reaching the nominal value of 200 at the measured current range.

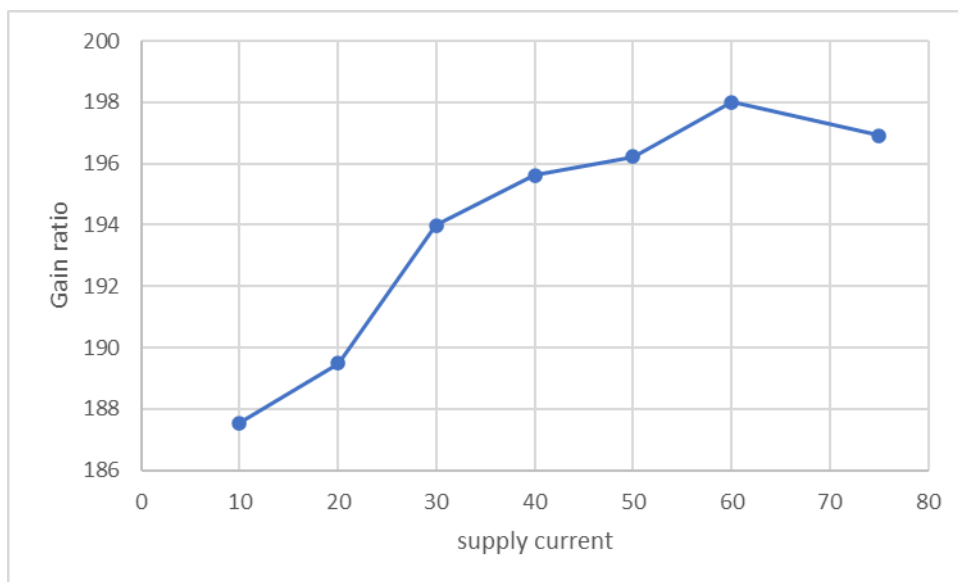


**Figure 2.20** Supplied current vs real voltage drop across busbar segment

**The error due to input offset voltage** has to be accounted for, before exploring the relation between amplifier 2 output and supply current. At 60 A supply, amplifier output averages at 174.9 mV while the average real voltage is 883  $\mu$ V. From the nominal gain of 200, the amplifier output should follow as

$$(883 \mu\text{V}) \times 200 = 176.7 \text{ mV} \quad (2.3)$$

However, due to negative input offset voltage it remains at 174.9 mV. Subtracting the result of (2.3) from this output and dividing it by the gain ratio gives -8.9  $\mu$ V of input offset voltage. Since this value affects the whole measurement range, correction should be made to eliminate the corresponding error. In this analysis, it should be also noted that there was still some voltage on the busbar segment, despite no supply current being given. This can be explained by the various sources of noise in the circuit. Evidently, temperature effects on input offset V and gain were also disregarded, as amplifier temperature change is negligible due to constant ambient temperature.

Correcting across the supply range for the input offset voltage, Figure 2.21 is obtained. It is clear that with correction, the gain values are much closer to the tolerance range of 200 +/- 0.2%

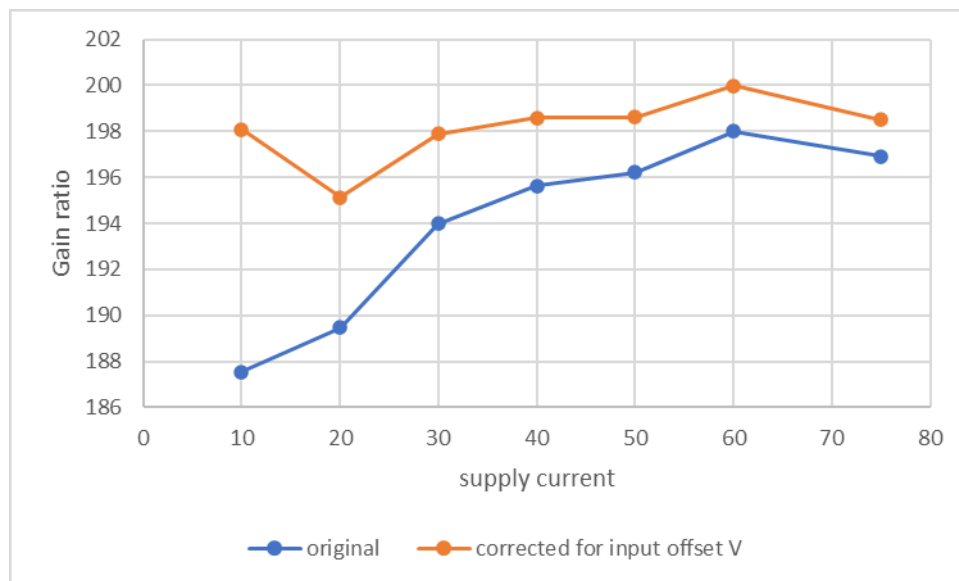


**Figure 2.21** Supplied current vs real voltage drop across busbar segment

**Next source of error is the temperature drift** of the Al busbar resistance. Since the other supply values could not induce a significant temperature increase until steady state, only 75 A supply case will be explored for this error type. Figure 2.22 shows a parabolic temperature increase in busbar, while the voltage outputs show a weak correlation, although in an increasing trend. The slight increases in the voltage signals are due to the changes in resistance of the busbar segment. This is by no means desirable, as a stable amplifier output is expected for constant current. However, it is inevitable in shunt resistors [4]. Despite a relatively large supply current of 75 A, the busbar only went from 27.2°C to 33.6°C. And remained SS at 33.6°C. Although it is a small difference to make an adequate analysis, an iteration will be made.

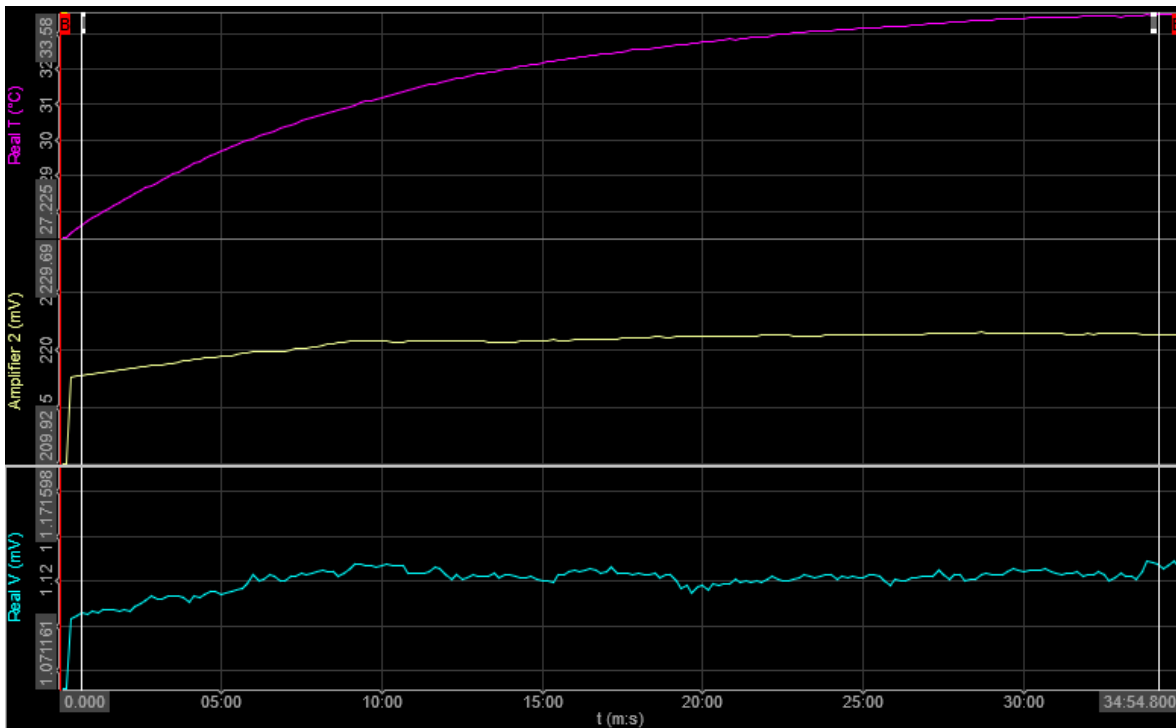


**Figure 2.22** Supplied current vs real voltage drop across busbar segment

Figure 2.23 depicts the ratio between amplifier output and supply current for the actual output data and for the calculated output data. It is noteworthy that this ratio is directly proportional to the resistance of the busbar segment. The calculated data was created using the temperature coefficient of Al, 0.00429 /K [15]. It is clear that the busbar resistance does not follow the formula

$$\frac{dR}{R} = \alpha \times dT \quad (2.4)$$

Although this can be due to other sources of error, material impurities are known to alter temperature coefficient. Calculating again with a correction coefficient of 1/1.35, one finds that an  $\alpha$  of 0.00317 /K better fits the measurement data (Figure 2.24).

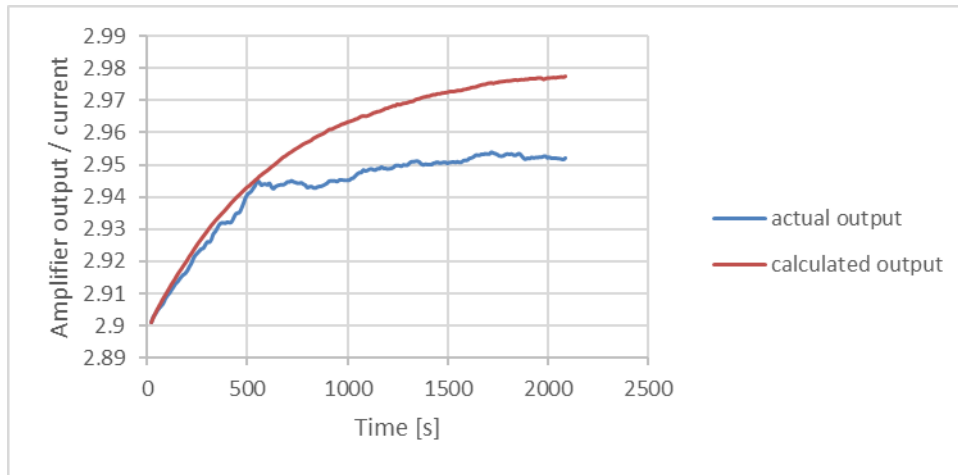


**Figure 2.23** Amplifier output – current ratio vs calculated output

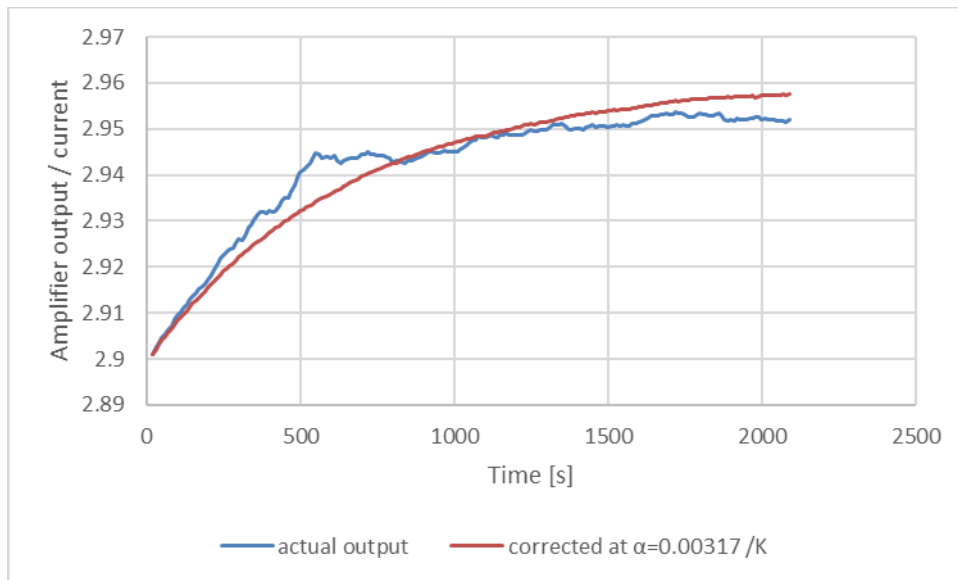


**Figure 2.24** Amplifier output – current ratio vs corrected calculated output

Another question in temperature monitoring was how accurate the thermistor would be. At Figure 2.25, roughly a temperature increase of 6 K was depicted showing both

outputs. With a difference of max. 0.4 K, the thermistor appears to be sufficiently adequate for temperature monitoring.

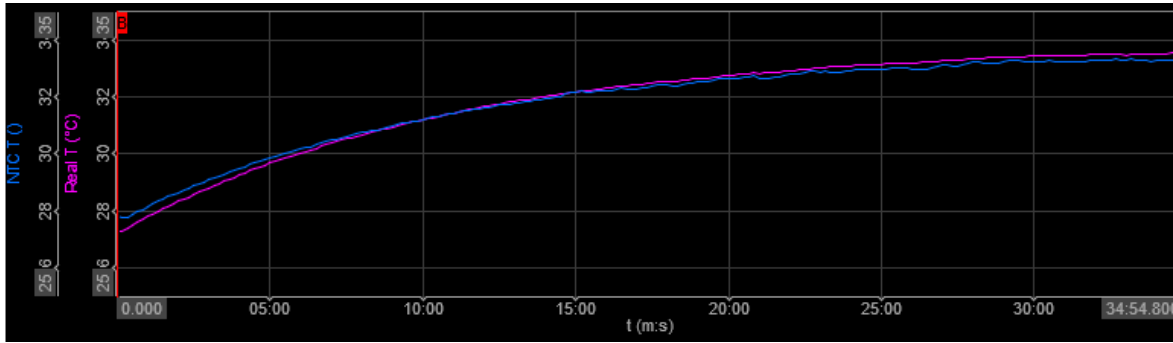


**Figure 2.25** Comparison of real temperature (thermocouple) and thermistor output

## 2.5 Calibration method

The module that is the subject of this study is to be serially produced. This means that there will be relatively short time for each module to be calibrated for current sensing. The available information during calibration will be limited. Supplied current will be known via testing devices. Real-time temperature will be monitored via the thermistor on the busbar. The last available information is amplifier output, which will be converted to digital signal to be sent to module microcontroller. As the amplifier output is the primary indicator for the magnitude of the electrical current, one needs to find a coefficient  $K$ ,

$$I = K \times v_{CSA} \quad (2.5)$$

Between the current and CSA (current sense amplifier) output. As the resistance of the busbar segment (shunt resistor) will change with temperature, a temperature coefficient of  $\alpha$  must be determined as well. (2.5) becomes,

$$I = K \times v_{CSA} \times (1 + \alpha \times dT) \quad (2.6)$$

The remaining significant error source is the input offset voltage of the CSA,  $v_{i,o}$ . If the temperature drift of  $v_{i,o}$  is ignored [9], its effect on the current function can be represented as gain times input offset voltage,  $G_{CSA} \times v_{i,o}$ . It follows,

$$I = K \times (v_{CSA} + G_{CSA} \times v_{i,o}) \times \left(\frac{1}{1 + \alpha \times dT}\right) \quad (2.7)$$

$v_{i,o}$  can be both negative and positive. Although it can vary within the given tolerance range in the TDS of CSA [9], it will be constant for a specific CSA specimen. A simple method for determining  $v_{i,o}$  is given as follows: As the amplifier output will be equal to  $G_{CSA} \times v_{i,o}$  when no current is supplied, this value can be calculated with the knowledge of  $G_{CSA}$  and available  $v_{CSA}$ . Clearly, very low noise presence is required for an accurate determination. Figure 2.26 introduces a calibration sequence to be performed during module tests. Following the determination of  $v_{i,o}$ , two consecutive tests will be performed to obtain  $K$  and  $\alpha$ . As the procedure is sequential, it is important to insert the obtained values into the algorithm before moving onto the next step. During the determination of  $K$ , it is important to select a supply current that is at the midpoint of the typical operating range of the module. Another important point is to keep the supply current for a short duration to prevent heating up the busbar, as at this stage, temperature effects are out of equation. At the final step, temperature coefficient  $\alpha$  is obtained by supplying a significant amount of current (ideally  $>200$  A) until a predefined temperature. Knowing the amplifier outputs and the temperatures at the two calibration points,  $\alpha$  is calculated according to the relation at (2.4).

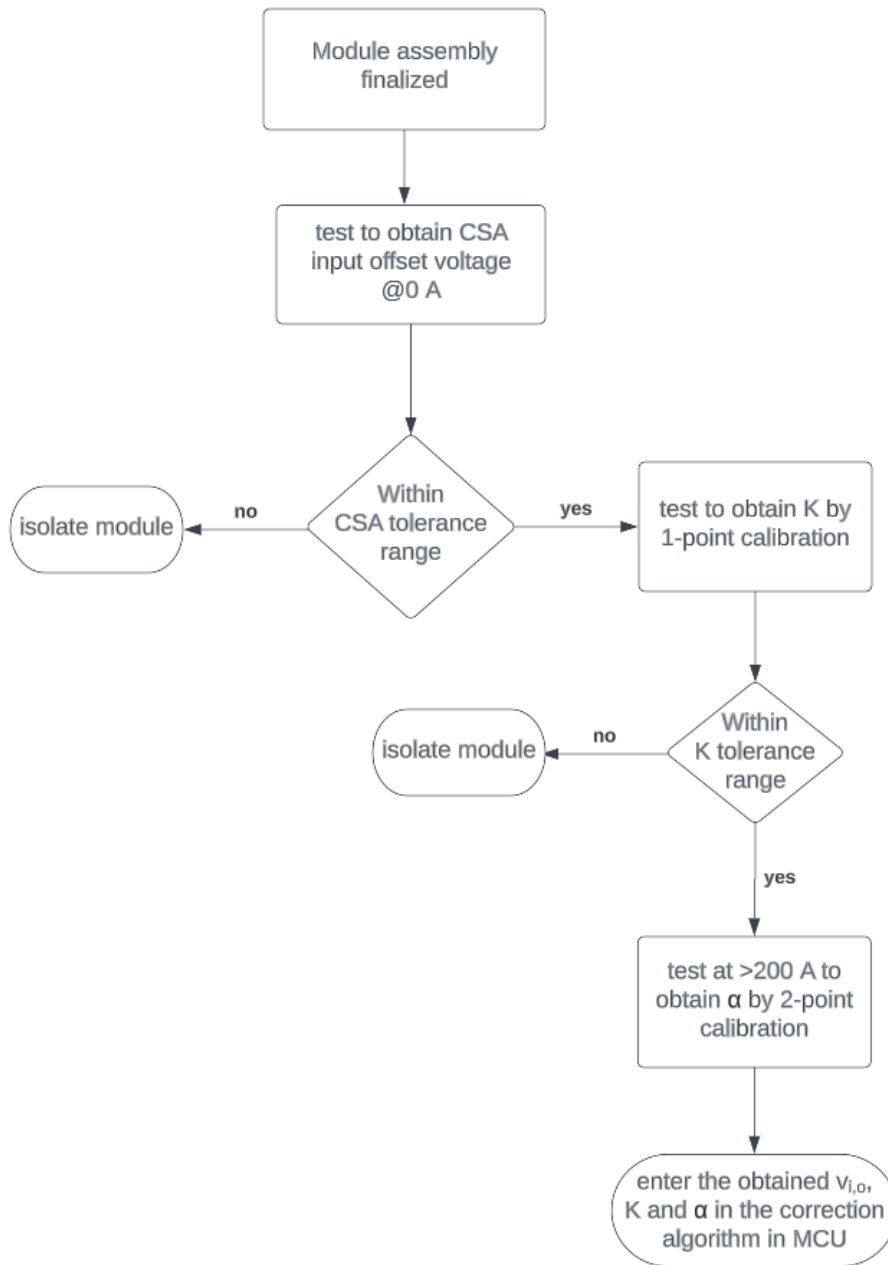


**Figure 2.26** Process flowchart of module current sensing calibration

### 3.RESULTS

Putting to work the method described at 3.5, K will be calculated using 1-point calibration at 40 A, which represents the midpoint of a plausible working range for the module. Knowing  $v_{i,o} = -8.9 \mu\text{V}$ ,

$$I = K \times (v_{CSA} + G_{CSA} \times v_{i,o}) \tag{2.8}$$

becomes

$$40 = K \times (117.7 + 200 \times (-0.0089)) \tag{2.9}$$

Gives  $K = 0.345 \text{ A/mV}$

Using K to calculate currents according to CSA outputs at points between 10 A and 75 A gives

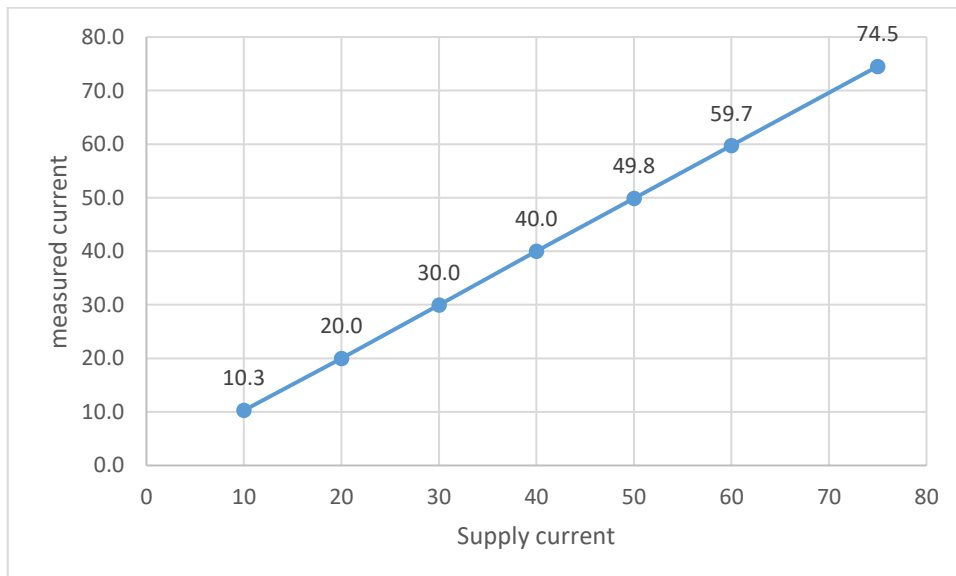


**Figure 3.1** Measured currents using the calibration procedure at various supply currents

Table 3.1 below summarizes the percentage errors at all the supply points. Apart from the smallest and highest current values all errors are below 0.5%. The high errors at the end points can be explained with the high impact of resident noise at the low end,

and the slightly increased temperature at the high end. The calibration for temperature effect will be presented next.

**Table 3.1** Percentage errors at supply currents

Supply current	Percentage error [%]
10	-2.85
20	0.11
30	0.16
40	0.04
50	0.31
60	0.47
75	0.63

As mentioned in Chapter 3, only 75 A was sufficient to cause a considerable temperature increase at the busbar segment. This time, instead of using the  $\alpha$  that was calculated by curve fitting, a two point calibration will be used to determine it, as instructed in the calibration method. For this the initial temperature of 27.4°C is selected as 1st point, and 33°C as the second. This resulted in a temperature coefficient of 0.0029 /K. Having determined K previously and substituting for  $v_{CSA}$ ,  $G_{CSA}$ ,  $v_{i,0}$  and  $\alpha$ , it is possible to calculate I throughout entire dataset.

$$I = K \times (v_{CSA} + G_{CSA} \times v_{i,0}) \times \left( \frac{1}{1 + \alpha \times dT} \right)$$

As the calibration Figure 3.28 shows the current trends with busbar temperature for calibrated and non-calibrated current sensing. From the trends, it is clear that the increasing trend of the non-calibrated current is suppressed by the calibration formula. Table 3.2 shows that the calibration procedure manages to keep the error under 1% for the entire range. Further trials at bigger temperature intervals are certainly necessary.

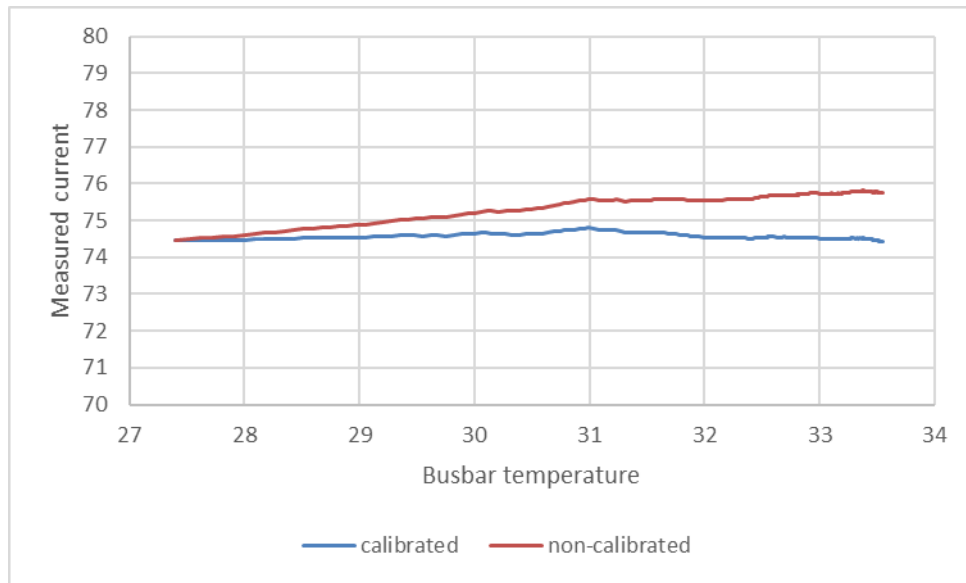


**Figure 3.2** Measured currents using the calibration procedure at the temperature interval

**Table 3.2** Percentage errors throughout the temperature interval

Busbar temperature	Percentage error [%]
28	-0.7
29	-0.61
30	-0.45
31	-0.26
32	-0.62
33	-0.66

## SUMMARY

This thesis study aimed to provide a proof-of-concept for a busbar-based shunt resistor current sensing method for a supercapacitor module. In greater context, the main desire was to find a simple and cost-effective current sensing solution for the module under development. As a result of the examination of the existing technologies on the market, current sensing with shunt resistors were the most suitable choice for its reliability, low cost and ease of implementation. Further simplification of this method is using a portion of the circuit as the current sensing shunt resistor. Due to being on the low voltage side of the module circuit, the negative terminal busbar was selected as the shunt resistor. Two main advantages for using an existing element of the circuit are no added cost and not increasing the total resistance of the module.

To verify that an aluminum busbar could act as a reliable shunt resistor at different currents, simulations were done at both steady-state and transient cases. The simulation results showed that the busbar provided a linear relation between voltage and current at different supply currents, only changing its resistance with temperature, as expected. In the end it was understood that by correcting for temperature effects, it was possible to use this busbar as a current sensing shunt resistor.

Next step was testing with actual parts. It was not possible to use the module in tests as it was still under development, therefore a partial assembly was used. The scope was limited to current sensing circuit validation and observation of temperature effects. Several tweaks to the circuit was necessary to properly run it, and utmost care was given to eliminate noise. In order to provide reference values to compare with the current sensing outputs, busbar voltage and temperature were simultaneously monitored by a DAQ. The results showed that there was a linear relation between CSA output and the supply current, and it was possible to correct for temperature effects by using calibration procedure. Based on the test results and taking into account the serial production conditions for the module, a calibration procedure was devised (Figure 3.26). The procedure was implemented in Chapter 4 with results under 1% errors except for the lowest supply current.

It should be noted that further testing and validation should be made to cover a wider range of module operating conditions, such as high-current pulses and power cycling, as well as testing for the entire output range for both charging and discharging. Another investigation area are the remaining sources of error on the sensing circuit, such as thermo-voltages, skin effect, and EMI. The long-term thermal fatigue effect on the busbar and a need for re-calibration is also relevant research field. All in all, this thesis

study provided promising results for the proposed solution, with the potential of providing a cost-effective and simplistic current sensing for supercapacitor modules. This in turn can improve the SoH monitoring, hence increasing the performance and lifetime of the devices.

## KOKKUVÕTE

Selle lõputöö eesmärk oli tõestada kontseptsioon voolulati põhise šunditakisti voolu mõõtmise meetodi kohta superkondensaatori mooduli jaoks. Laiemas kontekstis oli peamine soov leida arendatavale moodulile lihtne ja kulutõhus vooluanduri lahendus. Turul olemasolevate tehnoloogiate uurimise tulemusena osutus šunttakistitega vooluandur oma töökindluse, odavuse ja kasutusmugavuse poolest sobivaimaks. Selle meetodi edasiseks lihtsustamiseks kasutatakse šunditakistit vooluahela osana. Šunditakisti asukohaks valiti mooduli negatiivne voolulatt, kuna see on kõige madalama pinge juures. Olemasoleva vooluahela elemendi kasutamise kaks peamist eelist on lisakulude puudumine ja mooduli kogutakistuse mitte muutumine.

Et kontrollida, kas alumiiniumlatt võib erinevatel vooludel töötada usaldusväärse šunditakistina, tehti simulatsioone nii püsiseisundi kui ka siirdejuhtumite korral. Simulatsiooni tulemused näitasid, et voolulatil oli lineaarne seos pinge ja voolu vahel erinevate toitevoolude korral, muutes ootuspäraselt ainult selle takistust temperatuuriga. Lõpuks jõuti arusaamisele, et temperatuuri mõjusid korrigeerides on võimalik seda voolulati kasutada šunditakistina.

Järgmine samm oli testimine füüsiliste komponentidega. Moodulit ei olnud võimalik testides kasutada, kuna see oli alles väljatöötamisel, mistõttu kasutati osalist komplekti. Testimise fookus piirdus vooluanduri ahela valideerimise ja temperatuurimõjude jälgimisega. Vooluahela korralikuks toimimiseks oli vaja teha mitu muudatust ja müra kõrvaldamisele pöörati suurt tähelepanu. Et anda võrdlusväärtsi, mida saaks võrrelda vooluanduri väljunditega, jälgiti voolulati pinget ja temperatuuri andmete kogumise süsteemi abil. Tulemused näitasid, et voolumõõtmise võimendi väljundi ja toitevoolu vahel oli lineaarne seos ning temperatuuri mõju oli võimalik korrigeerida kalibreerimisprotseduuri abil. Katsetulemuste põhjal ja võttes arvesse mooduli seeriatootmise tingimusi, töötati välja kalibreerimisprotseduur (joonis 3.26). Protseduuri rakendati peatükis 4, mille tulemused olid alla 1% vigadega, välja arvatud madalaima toitevoolu korral.

Tuleb märkida, et tuleks teha täiendavaid katseid ja valideerimist, et katta rohkem erinevaid opereerimistingimusi, nagu kõrged vooluimpulsid ja võimsustsüklid, samuti kogu väljundvahemiku testimine nii laadimisel kui ka tühjaks laadimisel. Veel üks uurimisvaldkond on andurahela ülejäänud veaallikad, nagu termopinged, pinnaefekt ja elektromagnetilised häired. Asjakohane uurimisvaldkond on ka pikaajaline termilise väsimuse mõju voolulatile ja vajadus uuesti kalibreerida. Kokkuvõttes andis see lõputöö pakutud lahenduse jaoks paljulubavaid tulemusi, mis võimaldasid pakkuda

superkondensaatorimoodulitele kulutõhusat ja lihtsustatud vooluandurit. See võib omakorda parandada mooduli seisundi hindamist, suurendades seadmete jõudlust ja eluiga.

## LIST OF REFERENCES

- [1] D. Torregrossa, M. Paolon, "Modelling of current and temperature effects on supercapacitors ageing. Part II: State-of-Health assessment", *Journal of Energy Storage*, Volume 5, 2016, pp. 95-101.
- [2] L. Xinghua and Z. Mingkun, "Research on high-precision survey of supercapacitor ESR," 2011 International Conference on Electronics, Communications and Control (ICECC), Ningbo, China, 2011, pp. 1627-1630, doi: 10.1109/ICECC.2011.6066345.
- [3] "Using a PCB Copper Trace as a Current-Sense Shunt Resistor," ti.com, <https://www.ti.com/lit/pdf/sboa533> (accessed Mar. 15, 2023).
- [4] "The Current Transformer," Electronics Tutorials, <https://www.electronicstutorials.ws/transformer/current-transformer.html> (accessed Mar. 15, 2023).
- [5] P. Weßkamp et al., "High Performance Current Measurement with Low-Cost Shunts by means of Dynamic Error Correction," 18. GMA/ITG-Fachtagung Sensoren und Messsysteme 2016 2016-05-10 - 2016-05-11, doi: 10.5162/sensoren2016/3.4.4.
- [6] "Melexis MLX91209 Hall Effect Current Sensor," Mouser Electronics, <https://www.mouser.ee/new/melexis/melexis-mlx91209-current-sensor/> (accessed Mar. 15, 2023).
- [7] T. Koseki, Y. Takada, H. Obata, Y. Hayakeyama, W. Teppan and E. Favre, "Measurement and modeling of nonlinear magnetic core characteristics of a fluxgate direct current sensor for wide-range current monitoring," 2009 International Conference on Electrical Machines and Systems, Tokyo, Japan, 2009, pp. 1-6, doi: 10.1109/ICEMS.2009.5382643.
- [8] "Supercapacitor modules," Skeleton Technologies, <https://www.skeletontech.com/en/supercapacitor-modules> (accessed Mar. 15, 2023).
- [9] "Resistive Current Sensing: Low-Side vs. High-Side Sensing," All About Circuits, <https://www.allaboutcircuits.com/technical-articles/resistive-current-sensing-low-side-versus-high-side-sensing/> (accessed Mar. 18, 2023).
- [10] "INA240 –4-V to 80-V, Bidirectional, Ultra-Precise Current Sense Amplifier With Enhanced PWM Rejection," Texas Instruments, <https://www.ti.com/lit/gpn/INA240> (accessed Mar. 12, 2023).
- [11] E. Grundkötter, P. Weßkamp and J. Melbert, "Transient Thermo-Voltages on High-Power Shunt Resistors," in *IEEE Transactions on Instrumentation and Measurement*, vol. 67, no. 2, pp. 415-424, Feb. 2018, doi: 10.1109/TIM.2017.2775418.
- [12] Brandt, R., Neuer, G. Electrical Resistivity and Thermal Conductivity of Pure Aluminum and Aluminum Alloys up to and above the Melting Temperature. *Int J Thermophys* 28, 1429–1446 (2007). <https://doi.org/10.1007/s10765-006-0144-0>

- [13] "Calculating and simulating error in current sensing systems," Texas Instruments, [https://www.ti.com/lit/ml/slyp710/slyp710.pdf?ts=1683618763110&ref\\_url=https%253A%252F%252F](https://www.ti.com/lit/ml/slyp710/slyp710.pdf?ts=1683618763110&ref_url=https%253A%252F%252F) (accessed May 05, 2023).
- [14] D. W. Braudaway, "Behavior of resistors and shunts: with today's high-precision measurement capability and a century of materials experience, what can go wrong?," in *IEEE Transactions on Instrumentation and Measurement*, vol. 48, no. 5, pp. 889-893, Oct. 1999, doi: 10.1109/19.799641.
- [15] Giancoli, Douglas C., *Physics*, 4th Ed, Prentice Hall, (1995).
- [16] "Bourns CSM2F-8536-L025J00," Mouser Electronics, <https://www.mouser.ee/ProductDetail/Bourns/CSM2F-8536-L025J00?q=stqOd1AaK7%2FfaVpxy2dOng%3D%3D> (accessed May. 18, 2023).